INTERFACIAL SELF-ASSEMBLIES OF SURFACTANTS AT WATER-OIL INTERFACES

A Thesis
IN
Mechanical Engineering

Presented to the Faculty of the University
of Missouri–Kansas City in partial fulfillment of
the requirements for the degree

MASTER OF SCIENCE

by
HOUMAN HONARYAR

B. S., Amirkabir University of Technology (AUT), Tehran, Iran, 2019

Kansas City, Missouri
2021

INTERFACIAL SELF-ASSEMBLIES OF SURFACTANTS AT WATER-OIL INTERFACES

Houman Honaryar, Candidate for the Master of Science Degree

University of Missouri–Kansas City, 2021

ABSTRACT

The generation of novel synthetic materials with functionality and hierarchical ordering is a major focus of current studies in materials science and engineering. Self-assembling amphiphilic materials (such as lipids or surfactants) are an important subgroup of colloids and soft matter and are being used as an ideal candidate for such purposes due to quickly forming rich supramolecular structures across nanometer and micrometer length scales. The immiscible liquid-liquid interfaces which are constrained environment have proved to offer ideal platforms for such endeavors where surface-active nanoparticles or molecules can accumulate and self-assemble. In this thesis, we focus on self-assembly of surfactants which induce formation of nano- or microstructures at the interface between the aqueous solution of a surfactant (ionic or non-ionic) and a polar oil (such as oleic acid).

First, self-assembly of different types of surfactants (ionic vs. non-ionic) at immiscible water-oil interface is used for the newly emerged *liquid-in-liquid* 3D printing.

In this printing approach, the aqueous solution of surfactants and the oil constitute the printing phase and support liquid, respectively. Considering the low viscosity of aqueous solutions, the printed liquid constructs using this technique are significantly well-defined and relatively complex in shape. Interfacial rheology is utilized to understand viscoelastic properties of the interfacial layer made between the surfactant solution and oil phase. This gel-like material formed at the interface is robust enough that makes the printed liquid construct perfusable, enabling an injected solution to flow within its structure without any change in the shape and integrity of print. The kinetics of aggregate formation at the water-oil interface is also studied in two cases; when aqueous solution is stagnant (static) and in contact with oil phase and when the aqueous solution is flowing (dynamic) over oil phase. Then relevant models are established for these two conditions and the key aspects of formation of such structures are discussed. According to the proposed models, estimates for solubilization rate of oleic acid into aqueous solution are measured for both dynamic and static conditions. Subsequently, a computational simulation (dissipative particle dynamics) is performed to study the self-assembly behavior of each component (i.e. a cationic surfactant and a polar oil) in water. These self-assemblies behaviors are validated successfully based on the other experimental or simulation studies. Finally, mesoscopic simulation of water-oil interface with presence of all three components (surfactants/oil/water) provides us with an insight into dynamics and the underlying morphological pathway for the structure formation.

The significance of this work lies in the printing of low viscous solutions of self-assembling materials into relatively complex designs which is enabled by surfactant self-assemblies and can be of use in various applications such as fabrication of liquid electronics and novel media for encapsulation of cells. This printing approach can be easily applied for different types of surfactants (ionic and non-ionic), block copolymers, biocompatible surfactants, peptides, or proteins. With having relevant kinetic modelings coupled with validated computational simulation of the system, one will be able to tailor desired microstructured materials and properties by tuning the type and concentration of constituent components, and dynamics of the system (i.e. flow rate of aqueous solution).

APPROVAL PAGE

The faculty listed below, appointed by the Dean of the School of Computing and Engineering, have examined a thesis titled “Interfacial self-assemblies of surfactants at water-oil interfaces,” presented by Houman Honaryar, candidate for the Master of Science degree, and hereby certify that in their opinion it is worthy of acceptance.

Supervisory Committee

Zahra Niroobakhsh, Ph.D., Committee Chair
Department of Civil & Mechanical Engineering

Antonis P Stylianou, Ph.D.
Department of Civil & Mechanical Engineering

Stefan Lohfeld, Ph.D.
Department of Civil & Mechanical Engineering

CONTENTS

ABSTRACT iii

ILLUSTRATIONS ix

TABLES xii

ACKNOWLEDGEMENTS xiii

Chapter

1 INTRODUCTION 1

1.1 *Liquid-in-Liquid* 3D Printing 3

1.2 Importance of Research on Self-assembly Systems at Liquid-Liquid Interfaces 4

1.3 Experimental Materials Properties 6

1.4 Task Description 9

2 EXPERIMENTAL INVESTIGATION ON *LIQUID-IN-LIQUID* 3D PRINTING USING SURFACTANT SELF-ASSEMBLY 11

2.1 *Liquid-in-liquid* 3D Printing Using Surfactant Self-assembly 11

2.2 Interfacial Rheology 13

2.3 Results & Discussion 14

2.4 Conclusion 20

3 KINETIC STUDY 22

3.1 Calculation of OA Solubilization Rate 28

3.2 Conclusion 35
4 COMPUTATIONAL SIMULATION (DISSIPATIVE PARTICLE DYNAMICS) 36
4.1 DPD Parameterization 37
4.2 CPCl Phase Behavior in Water 40
4.3 OA Phase Behavior in Water 42
4.4 Ternary Phase Behavior 44
4.5 Conclusion 47
5 CONCLUSION AND FUTURE WORK 48
5.1 Conclusion 48
5.2 Future Work 49
REFERENCE LIST 51
VITA 63

ILLUSTRATIONS

Figure		Page
1	Schematic illustration showing arrangements of amphiphilic molecules in a micelle and the interacting forces. Reprinted from [1], Copyright (2011), with permission from Elsevier.	2
2	3D printing experimental setup.	12
3	Designed models for printing. a) 2D planar meandering channel. b) A helical structure.	13
4	Interfacial rheology experimental setup (left) and the schematic representation (right) of the DWR configuration demonstrating the position of the ring at the interface of the oil and the aqueous phases.	14
5	Printing of 2D planar designs (meandering channel) within an oil phase using aqueous solution of different types of surfactants. From left to right, the aqueous solutions contain SDS, F68, and CTAB.	15
6	Capability of printed liquid constructs to direct the perfusion of injected dye solution.	16
7	Printing of a helical structure using the aqueous solution of surfactant CPCl (425mM) within the oil phase. Very low amount of blue food colorant (≈ 0.2 wt%, Mc-Cormick) was added to aqueous solutions for easier visualization of the printed construct.	18

8 Printing of a helical structure using aqueous solution of different surfactant within the oil phase. From left to right, aqueous solutions contain CTAB, SDS, and Brij-35. Very low amount of blue food colorant ($\approx$ 0.2 wt%, Mc-Cormick) was added to aqueous solutions for better visualization of printed construct. 18

9 Schematic illustration showing the *liquid-in-liquid* 3D printing of a helical structure. 19

10 Interfacial rheology measurements: amplitude sweep (left) at 1 Hz and frequency sweep (right) measurements at fixed 0.1% strain and immediately after sample loading for CPCl aqueous solution (425 mM) and oil phase as shown in Figure 4. 20

11 Schematic of two major mechanisms of solubilization of oil molecules by surfactant aggregates. 25

12 Mass rates of OA into surfactant aqueous solutions over time for different concentration of CPCl in both static (left) and dynamic (right) conditions. The flow rate of aqueous solution in dynamic condition is Q= 100 ml/h. . 35

13 Representations of molecules (head group of CPCl represented with two beads: N & M, N representing the hydrophilic, and M the charged section and bulky nature of the surfactant). 39

14 CPCl self-assembly behavior in simulation based on conservative interactions reported in Table 7. 42

15 OA phase behavior in water in different concentrations. 44

16 Phase behavior of the ternary system for three scenarios with respect to interaction between CPCl and OA head groups (a_{MH} and a_{NH}). From left to right, the head groups of CPCl and OA are $\chi = 15$, $\chi = 25$, and $\chi = 50$. 45

17 Self-assembly behavior and structure evolution of ternary system (with an equimolar mixing ratio of CPCl and OA) for the case with χ=25. 46

TABLES

Tables		Page
1	Preferred geometrical structures of amphiphilic systems based on critical packing parameters. Reprinted from [1], Copyright (2011), with permission from Elsevier.	2
2	Surfactants molecular structures	8
3	Oils molecular structures	8
4	Mass flux of OA into different concentration of aqueous CPCl solution under static condition (i.e. no flow)	31
5	Mass flux of OA into aqueous phase with constant concentration (C=100 mM) at different flow rates under dynamic condition (i.e. flowing aqueous solution)	33
6	Mass flux of OA into aqueous phase with constant flow rate (C=100 ml/h) at different surfactant concentrations under dynamic condition (i.e. flowing aqueous solution)	33
7	DPD conservative interactions for beads of CPCl and water	41
8	DPD conservative interactions for beads of OA and water	43
9	DPD conservative interactions of all beads. χ denotes interaction between head groups of OA and CPCl.	45

ACKNOWLEDGEMENTS

First and foremost I would like to thank my advisor, Dr. Zahra Niroobakhsh, for being a reliable mentor, her support, and guidance throughout the process of completing this thesis. I would also like to thank my thesis committee members, Dr. Antonios P Stylianou and Dr. Stefan Lohfeld for taking time to be apart of this journey. I am also grateful to Dr. Julian Shillcock (Institute of Brain Mind, Ecole Polytechnique Federale de Lausanne) for development of code as well as advice and continuous help in computational simulation of my study (software can be found in Github). Last but not least, I would like to thank my friends and my family, my dad and my mom, for their moral support. Without them none of this would have been possible.

CHAPTER 1

INTRODUCTION

Amphiphilic molecules such as surfactants are comprised of a hydrophilic (water-liking) head and a hydrophobic (water-hating) tail. Surfactants depending on their head group charge can be classified as anionic, cationic, zwitterionic, or non-ionic [2]. Above a certain concentration, known as "Critical Micelle Concentration (CMC)", these molecules self-assemble into spherical micelles. With increase in concentration or presence of additives, co-surfactants, or other surface-active agents, these aggregates may undergo transition into a great variety of different structures; ellipsoidal micelles (rod-like or disk-like), vesicles, or lamellar structures [1, 3]. Entropic forces drive such behavior to minimize the contact of hydrocarbon tail with solvent (usually water). A convenient parameter for analyzing the resulting structures is a dimensionless number, known as the "critical packing parameter" (CPP) or "geometrical packing factor" (Figure 1);

$$\text{CPP} = v/a_0 l_c, \tag{1.1}$$

where a_0, v, and l_c are the optimum head group area, chain volume, and chain length of the molecule, respectively. The hydrophobic attraction between hydrocarbon chains causes the molecules to associate and tends to decrease the area per molecules (a_0), while the hydrophilic repulsion of the head groups behaves oppositely and causes the molecules to remain in contact with water [1]. These two forces determine the optimum head group area a_o at which the mean interaction free energy per molecule is at minimum. All of the preferred structures based on the geometric packing parameter are shown in Table1.

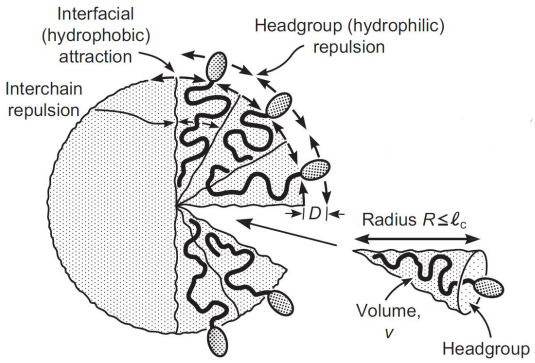

Figure 1: Schematic illustration showing arrangements of amphiphilic molecules in a micelle and the interacting forces. Reprinted from [1], Copyright (2011), with permission from Elsevier.

Table 1: Preferred geometrical structures of amphiphilic systems based on critical packing parameters. Reprinted from [1], Copyright (2011), with permission from Elsevier.

Critical packing parameter (CPP=$v/a_0 l_c$)	Preferred morphology	Illustration
0-1/3	Spherical Micelle	
1/3-1/2	Non-spherical (ellipsoidal) micelles	
1/2-1	Flexible bilayer, vesicle	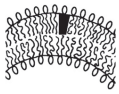
≈ 1	Planar bilayers, lamellar	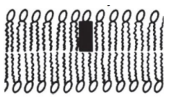
≥ 1	Inverted micelles	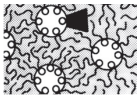

1.1 *Liquid-in-Liquid* 3D Printing

Three-dimensional (3D) printing, also known as rapid prototyping (RP), additive manufacturing (AM), or solid freeform fabrication, represents the fabrication of objects by successively adding materials layer by layer [4]. Over the past decade, 3D printing of soft materials with weak mechanical strength has been a challenge but benefits different fields ranging from tissue engineering to drug delivery devices [5]. Traditional solid layer-by-layer 3D printing for such materials is limited to constructing simple geometries with the help of support scaffolds which are challenging to be removed later. One potential remedy is *liquid-in-liquid* 3D printing in which these support structures are replaced with a liquid that is carefully selected based on its interaction with printing liquids [6]. To this end, the key factor is to precisely select the printing material and support phase to enable fabrication of 3D constructs with complex structural features by preventing the collapse of the soft materials after extrusion [7].

In the most common variant of *liquid-in-liquid* 3D printing technique, rheological behavior of the support liquid plays the most significant role. The support liquid yields and fluidizes at the location of moving dispensing tip. Upon the removal of stress, the support liquid rapidly resolidifies and holds the dispensed material in place until the solidification of printed construct is complete through crosslinking or gelation [7]. The materials that constitute support baths with such rheological properties are limited to microparticle gels [8], densely packed oil-in-water emulsions [9], and biopolymer solutions [10]. To name a few methods reported in the literature with this approach, Hinton et al. printed complex structures by embedding a hydrogel within a secondary hydrogel that

serves as temporary, thermoreversible, and biocompatible support [11]. Bhattacharjee et al. also used the same approach with a granular medium to print different biocompatible hydrogels into very complex architectures [12]. Noor et al. printed high-resolution thick, vascularized, and perfusable cardiac patches that completely match the immunological, cellular, biochemical, and anatomical characteristics of the patient [13]. What makes these approaches valuable and challenging is the fact that weak mechanical properties of printing soft materials is tackled by having a support medium, hence architectures with different designs and features are fabricated [7].

1.2 Importance of Research on Self-assembly Systems at Liquid-Liquid Interfaces

Among all reported *liquid-in-liquid* 3D printing techniques, there are only limited approaches which use liquid-liquid interfaces to induce or control the interaction of printing phase and support phase in order to print soft materials [6, 14, 15]. In these studies, the printed constructs are fabricated in form of either liquid droplet networks [15, 16] or continuous self-supporting liquid constructs [6, 14]. These reported printing approaches are based on the formation of interfacial membranes [6], interfacial jamming of surface-active nanoparticles [14], or formation of lipid bilayers at the liquid-liquid interfaces [15, 16].

Even though there is limited focus on liquid-liquid interfaces for additive manufacturing, these interfaces are mostly used for other purposes such as substance separation [17, 18], transportation [19, 20], nucleation [21], and organization of rich assemblies [22]. To optimize the functionality of these processes, liquid-liquid interfaces are usually required to be stabilized, mostly by generation of nano- or microstructures [23, 24]. In such

stabilized interfaces, each liquid phase contains interactive components such as colloids, particles, surfactants, macromolecules, and polymers which induce a rapid mechanism, giving rise to the formation of structured interfaces. Examples of these mechanisms include interfacial polymerization [25–27], gelation in hydrogels [28, 29], chemical reactions [30], and self-assembly of amphiphilic molecules [14, 31, 32]. Recently, the *in situ* formation of such structured interfaces has become a new trend since bulk fabrication of such interfaces usually yields no control over length scale, composition, and homogeneity [31, 33, 34]. Furthermore, the *in situ* fabrication of structured interfaces has proved to be quick and convenient while providing exceptional freedom for precise generation of localized multifunctional membranes at the prescribed location, unlike traditional bulk fabrication [25, 26].

To the best of our knowledge, there has not been any study regarding the use of surfactant self-assembly to stabilize liquid objects in *liquid-in-liquid* 3D printing. Self-assemblies of amphiphilic molecules at the interface have been primarily used for conventional bulk applications such as foams [35], solid dispersions [36], and emulsions (i.e. macroemulsions, nanoemulsions, and microemulsions) [3]. They, however, are recognized as promising candidates for *in situ* fabrication of stabilized, structured interfaces due to the spontaneous formation of various morphologies with spanning length scales from nano- to micrometers as well as striking rheological properties [24,33,37]. In biomaterials field, these interfacial self-assemblies made by amphiphilic biomolecules such as lipids, saccharides, peptides, and proteins have been used as *in situ* bottom-up approaches [38], for generation of asymmetric droplet-based vesicles in microfluidics [39], fabrication of

biomimetic membranes [40,41], nanostructured soft sacs [31,32], bioprinting of patterned cellular constructs [15, 16], and immobilization of cells in a privileged environment [42]. In another study, Niroobakhsh et al. have utilized the building blocks made by micellar-to-lamellar transition for the rapid fabrication of self-supporting structures [24]. In their study, the *in situ* self-assembly was navigated by manual injection of one amphiphilic-containing liquid phase (aqueous solution of surfactant) into the second one (fatty acid), leading to smooth nanostructured film formation [43]. The self-assembly structures in such surfactant systems are soft and flexible due to the weak secondary bonding, enabling them to quickly change under fluctuations (i.e. flow) through adjusting the nonequilibrium forces [1,44]. This behavior is favorable compared to self-assembly systems of rigid colloids (i.e. surface-active nanoparticles and macromolecules) in which stabilization of interface is achieved primarily by an irreversible close-packed monolayer [1,45–47]. Amphiphilic molecules (such as surfactants) have been used in many practical applications including membrane fabrication, foams [35], solid particles dispersion [36], and emulsions (i.e. macroemulsions, nanoemulsions, and microemulsions) [3], because of their capability to stabilize the interface between two liquids [14, 25].

1.3 Experimental Materials Properties

Here, in this study and for *liquid-in-liquid* 3D printing, we used all types of surfactants except for zwitterionic types. As cationic surfactants, we used cetylpyridinium chloride (CPCl, Sigma Aldrich) and hexadecyltrimethylammonium bromide (CTAB, Sigma Aldrich) which are the most common catanionic surfactants [48]. For anionic surfactants,

sodium dodecyl sulfate (SDS, Sigma Aldrich) and for nonionic surfactants, Pluronic F68 (F68) or Brij-35 (Sigma Aldrich) are used, respectively (Table 2). Aqueous solutions of CTAB and CPCl were obtained at concentration of 300 mM and 425 mM, respectively while aqueous solutions of Pluronic F68, Brij-35, and SDS were prepared with the concentration of 25 wt%. Aqueous solutions were prepared using purified, deionized water and experiments were performed at room temperature, 21.5 - 23.5^{o}C. Oleic acid (OA, technical grade 90%) and castor oil (CO, reagent grade 100%) were obtained from Alfa Aesar and a mixture with volume ratio of 1:1 was used as the oil phase. The molecular structures of surfactants and oils used in this study are provided in Table 2 and Table 3, respectively.

Table 2: Surfactants molecular structures

Surfactant name	Formula	Molecular structure
Cetylpyridinium chloride (CPCl)	$C_{21}H_{38}ClN.H_2O$	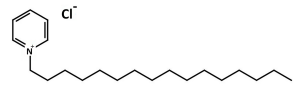
Hexadecyltrimethylammonium bromide (CTAB)	$C_{19}H_{42}BrN.H_2O$	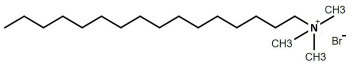
Sodium dodecyl sulfat (SDS)	Na $C_{12}H_{25}SO_4$	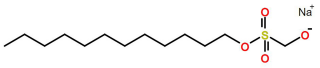
Polyoxyethylene (23) lauryl ether (Brij-35)	$(C_{18}H_{35}(OCH_2CH_2)_nOH$ n≈20	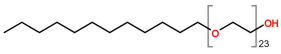
Pluronic F68 (Poloxamer 188)	$HO(C_2H_4O)_x(C_3CH_6O)_y(C_2H_4O)_zOH$	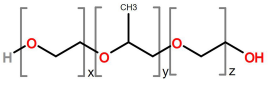

Table 3: Oils molecular structures

Oil name	Formula	Molecular structure
Oleic acid (OA)	$C_{18}H_{34}O_2$	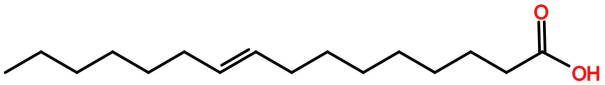
Castor oil (CO)	$C_{57}H_{104}O_9$	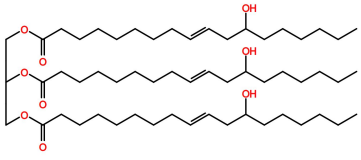

1.4 Task Description

In this thesis, self-assembly of surfactants is used in *liquid-in-liquid* 3D printing for stabilizing the immiscible water-oil interface through formation of supramolecular aggregates. This approach allows for structuring low viscous aqueous solutions into well-defined architectures within an oil phase. Patterning such low-viscous solutions into predefined structures has been impossible in both traditional additive manufacturing techniques and *liquid-in-liquid* 3D printing methods.

Printing these liquid architectures is enabled by self-assembly of surfactants during a nonequilibrium *in situ* process, thus kinetics play a critical role when it comes to modulating the self-assembly structures or incorporation of specific functions into such self-assembly systems [49]. Therefore, a kinetic study is conducted in this study to provide the insight into solubilization mechanism, dynamics, kinetics, and interaction between constituent components [50, 51]. This study allows us to precisely control and improve the formation of self-assembly for applications such as *liquid-in-liquid* 3D printing. For a system that consists of water/surfactant/polar oil, a variety of kinetic models have been proposed, each of which has its own advantage with respect to the condition and application of the system [51]. Different kinetics models will be assessed for the system to determine the one which correlates best with experiments and hence allows studying dynamics of structure formation at the interface. Two relevant kinetic models will be then established for the system in two conditions; when the aqueous solution is stagnant and when the aqueous solution is flowing in an oil phase which better models *liquid-in-liquid* 3D printing.

Formation of any nano- or microstructure by self-assemblies is associated with the synergistic effect of various intermolecular non-covalent interactions (i.e. hydrogen-bonding, electrostatic, hydrophobic), and therefore, thermodynamics is the key drive for the process of self-assembly formation [52]. Having a good understanding of underlying thermodynamics can help us to predict desired structures. To complement the experimental results for our ternary system (surfactant/water/polar oil), computer simulations are powerful tools to study the dynamics in micro-mesoscopic scale and can be used to predict and explain the thermodynamic properties as well as resulting microstructures [50]. In the literature, a variety of computer simulation methods have been used for this purpose including molecular dynamics (MD) and quantum dynamics which proved to be powerful for the investigation of interactions between molecules and atomic-scale calculation [53]. However, the time and length scale of these methods have hampered their wide applications for simulating systems with large scales. However, dissipative particle dynamics (DPD) as an alternative mesoscopic method has emerged to allow for the study of microstructures and thermodynamic properties up to the mesoscopic time and length scale [54,55]. Dissipative particle dynamics (DPD) as a mesoscopic simulation technique is used in this study to provide insight into dynamics and the underlying morphological pathway for the microstructure formation.

CHAPTER 2

EXPERIMENTAL INVESTIGATION ON *LIQUID-IN-LIQUID* 3D PRINTING USING SURFACTANT SELF-ASSEMBLY

It has shown previously that when an aqueous solution of a cationic surfactant (CPCl) is dispensed into an oleic acid reservoir, microstructures form at the water-oil interface and proved to stabilize different liquid shapes [24, 56]. The underlying phenomenon in this system is that the CPCl and oleic acid molecules interact at the water-oil interface, forming viscoelastic assemblies of surfactants [24, 43]. Results of this experiment laid the foundation for using this system in *liquid-in-liquid* 3D printing and to expand the research to other types of surfactants (anionic and nonionic).

2.1 *Liquid-in-liquid* 3D Printing Using Surfactant Self-assembly

Liquid structures were printed in the oil phase using a home-assembled 3D printer consisting of a liquid dispenser (Ultimus V high precision, Nordson efd) attached to a three linear translation stage (MTW Create, MakerToolsWorker). This translation stage coordinates the motion of the pneumatic syringe of liquid dispenser along programmed paths controlled by G-code commands (Figure 2).

2D meandering channels and helix models were generated using a MATLAB code (Figure 3). Prior to 3D printing, aqueous solutions of surfactants were drawn into a 30 cc plastic syringe (Nordson efd). In the pneumatically driven setup, the piston sits between the aqueous solution and the inlet of the pressurized air, generating a stable constant

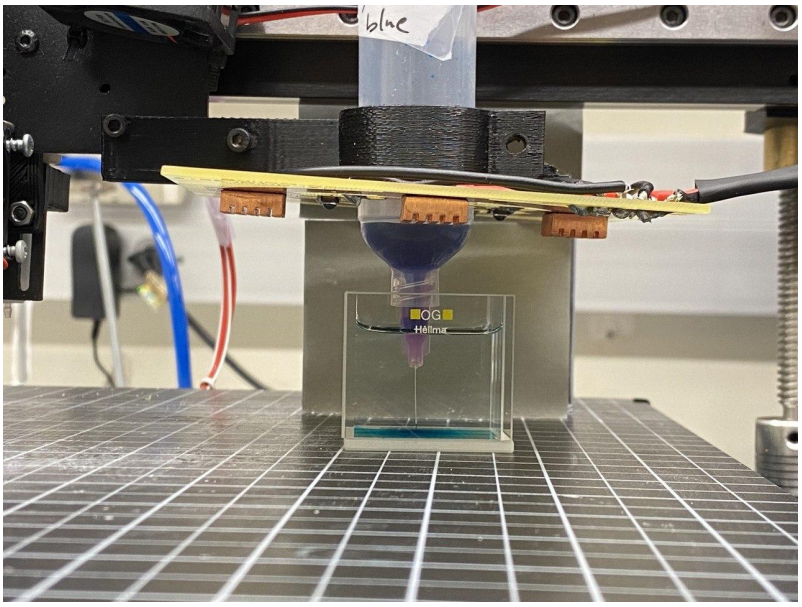

Figure 2: 3D printing experimental setup.

injection rate through the needle. The aqueous phase was injected at constant injection rates into the oil phase through print heads (needles) with internal diameters of 0.41 mm (22G, Nordson efd). For printing bath, a glass cuvette (30 mm$\times$30 mm$\times$30 mm, Hellma) or a petri dish (D = 5 or 10 cm, VWR) is used. The velocity range for lateral movement of print head were 0.8-1.2 cm/s, and the aqueous surfactant solution was injected with an applied pressure of 0.1-0.5 psi.

The velocity range for lateral movement of print head were 0.8 and 1.2 cm/s for both meandering channel and helix prints, respectively and the surfactant aqueous solutions were injected with an applied pressure of 0.1 or 0.2 psi, respectively. The injection rate corresponding to this range of applied pressures was measured to be $\sim$ 55-120 ml h^{-1} using two methods (suggested by liquid dispenser manufacturer): 1) by filling a volumetric flask and visually marking the time at which flask was filled using a timer, and 2)

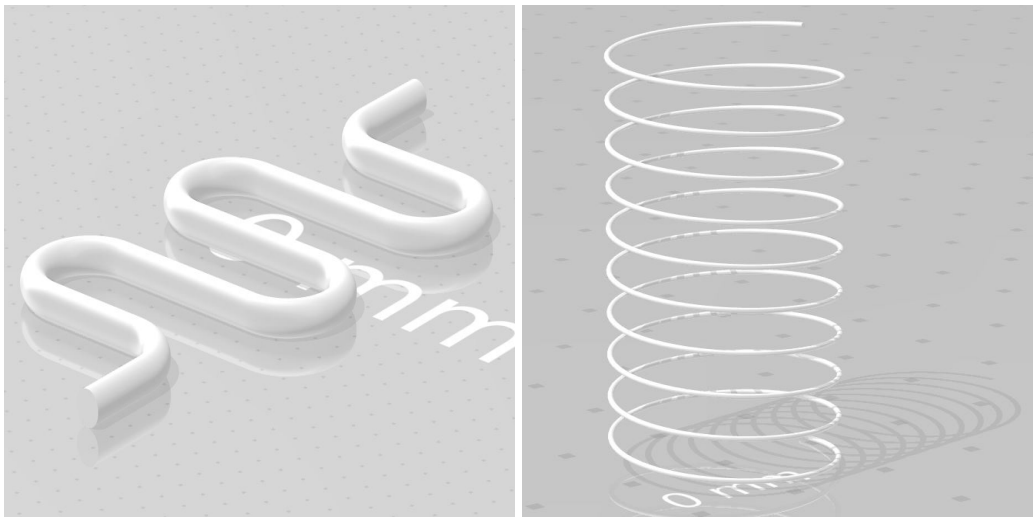

Figure 3: Designed models for printing. a) 2D planar meandering channel. b) A helical structure.

setting the liquid dispenser to do timed dispenses of 1 s and then measure the volume of each dispense by weighing each dispense and then convert the mass of the dispense into the volume.

2.2 Interfacial Rheology

The printing process is followed by rheological measurements which are crucial to evaluate viscoelastic behavior of the water-oil interface and to investigate any change in microstructure of the interface. For this printing approach to be successful, gel-like materials should develop at the interface of dispensed aqueous phase and oil and hence, the interfacial rheology will help us to confirm the presence of microstructure and gel-like material. A stress-controlled rheometer Discovery Hybrid Rheometer-3 (DHR3, TA Instruments) was used to carry out the rheological measurements (Figure 4). The aqueous solutions were loaded into the sample trough. Close visual inspection and axial testing

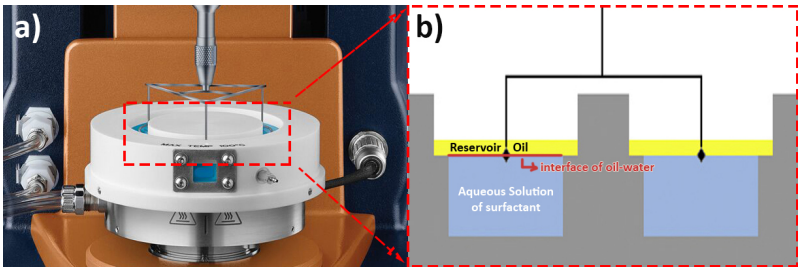

Figure 4: Interfacial rheology experimental setup (left) and the schematic representation (right) of the DWR configuration demonstrating the position of the ring at the interface of the oil and the aqueous phases.

were utilized to determine the interface for performing the interfacial measurement. Once a significantly different axial forces was sensed by instrument and the contact of ring with interface was confirmed through visual inspection, the ring was lowered 500 μm according to the instrument instruction. Then, the oil phase was gently added on the top of the aqueous phase using a needle to minimize the perturbation of the interface. The linear viscoelastic region was determined by an amplitude sweep test and a specific strain within that region was selected for subsequent frequency sweep test. The frequency sweep measurements were performed at fixed 1% strain which is within linear viscoelastic region.

2.3 Results & Discussion

Using the printer setup described earlier, we used the aqueous solution of three types of surfactants; CPCl (cationic), SDS (anionic), and Pluronic F68 (nonionic). First, a 2D planar design, i.e. a meandering channel is printed using aqueous solution of the surfactants. This design is considered to be complex due to the extreme curvatures and the short distance between each threads. The results are shown in Figure 5. All the printing

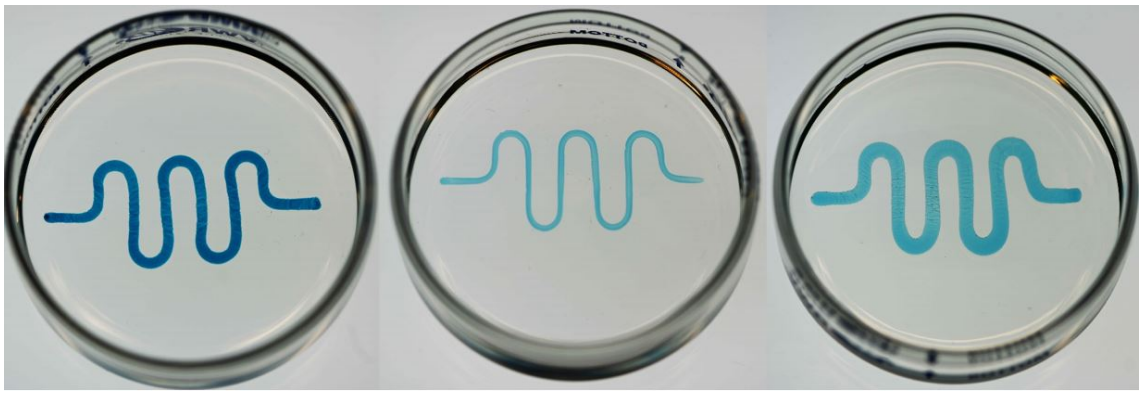

Figure 5: Printing of 2D planar designs (meandering channel) within an oil phase using aqueous solution of different types of surfactants. From left to right, the aqueous solutions contain SDS, F68, and CTAB.

parameters (i.e. printing speed and channel design) as well as physical parameters (i.e. injection rate and composition of the oil phase) were kept constant for all surfactants. The difference in the thickness of printed channels is associated with different viscosities of the aqueous solutions since a consistent applied pressure (hence injection rate) is used for printing. For the case of ionic surfactants (i.e. CPCl, CTAB, and SDS), the printed liquid constructs remained stable for over 4 hours without any change in integrity or shapes. For Pluronic F68 as the nonionic surfactant, the printed meandering channel disassembles after about one minute, most likely due to the weaker interfacial materials that form at the water-oil interface. However, given the fact that the printing material has low, water-like viscosity, the construct is printed with great precision and excellent quality.

Printed liquid constructs even showed to be capable of directing a flow along the structure without any change in shape and integrity of printed structure. Figure 6 shows how printed liquid structure is accommodating the perfusion of the injected dye solution

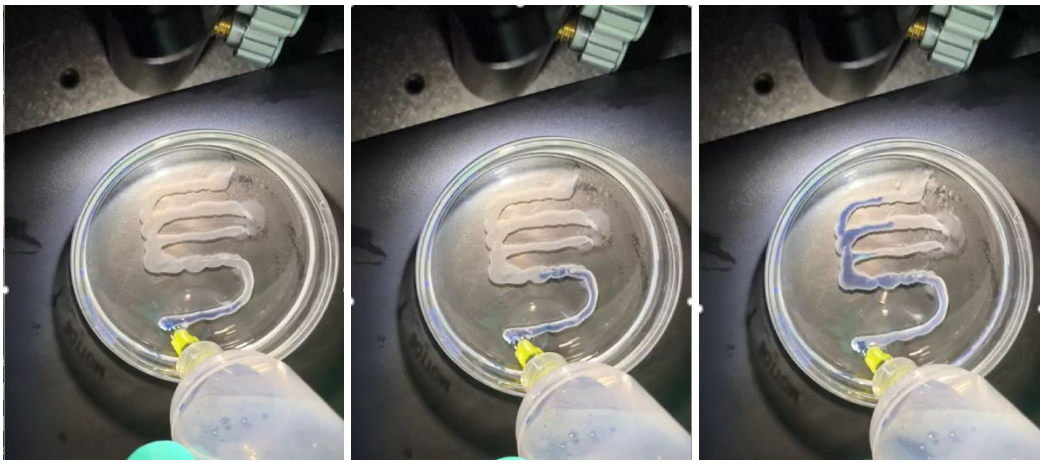

Figure 6: Capability of printed liquid constructs to direct the perfusion of injected dye solution.

without any change in its shape. This feature can be of interests in applications where certain process is required to occur within a predefined liquid architectures such as reaction vessels, liquid electronics, novel media for the encapsulation of cells [14].

In the next step, a 3D design with overhanging features such as a 4-cm-long spiral-shaped structure, about 8 mm in diameter is printed. For the case of CPCl solution (425 mM), the printed helical structures were found to be incredibly stable and more robust, exhibiting no visible changes for about two minutes (Figure 7) which indicates the potential of the approach to be used for printing more complex structures. After this time, the density difference between dispensed aqueous solution and oil phase causes the printed helical construct to either fall or break up into droplets which results in its deformation. In other cases, the printed structure breaks into droplets (for CTAB) or it starts to fall or float much faster (for SDS and Brij-35). These observations are most likely due to less surface activity of surfactants or their lower concentration (Figure 8). According to previous study

and specifically for CPCl solution, we hypothesize that once the aqueous phase comes into contact with the oil phase during printing, CPCl micelles undergo a morphological transition from micelles to lamellar [24]. This transition and formation of self-assembly at the interface is due to interaction between OA and surfactant molecules once the aqueous surfactant solution is injected into the oil bath. Critical packing parameter (CPP), a parameter for analyzing the resulting structures, as explained in Introduction Chapter, is used to account for such morphological transition. In fact, when CPCl encounters oleic acid, due to the dilution of CPCl surfactant molecules via oleic acid association, a change in critical packing parameter from CPP=1/3 to CPP$\approx$1 occurs which is satisfied by the lamellar morphology. Figure 9 shows the schematic representation of self-assembly of surfactants at the interface which enable the fabrication of liquid architectures within an oil phase.

Surfactants self-assembly at the interface usually results in rheological complexity at the interface, hence we need to describe the mechanical response of the interfacial materials. Figure 10 shows the amplitude sweep and frequency sweep measurements for the interfacial materials formed between the oil phase and aqueous CPCl solutions (425 mM). Based on the amplitude results, there is a linear viscoelastic region where both moduli (storage G' and loss G'') remain constant and insensitive to shear strain (deformation). The onset of 5% deviation from the constant values occur at a strain of 4% which is also considered as the limit of deformation without destroying the structure of the sample. Hence a strain within this linear region (1%) is selected for the subsequent frequency sweep measurements. Frequency sweep measurement results reveal that there is a larger

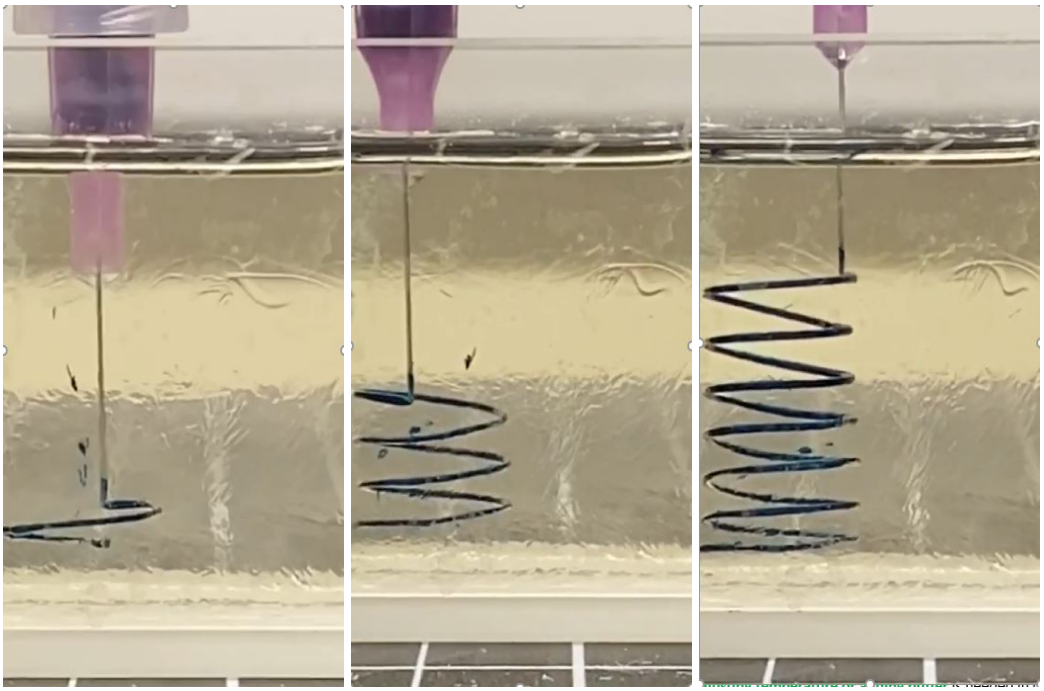

Figure 7: Printing of a helical structure using the aqueous solution of surfactant CPCl (425mM) within the oil phase. Very low amount of blue food colorant ($\approx$ 0.2 wt%, Mc-Cormick) was added to aqueous solutions for easier visualization of the printed construct.

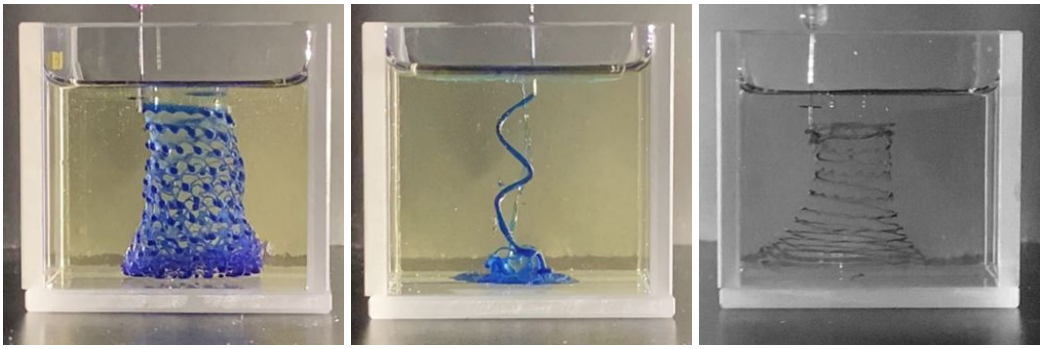

Figure 8: Printing of a helical structure using aqueous solution of different surfactant within the oil phase. From left to right, aqueous solutions contain CTAB, SDS, and Brij-35. Very low amount of blue food colorant ($\approx$ 0.2 wt%, Mc-Cormick) was added to aqueous solutions for better visualization of printed construct.

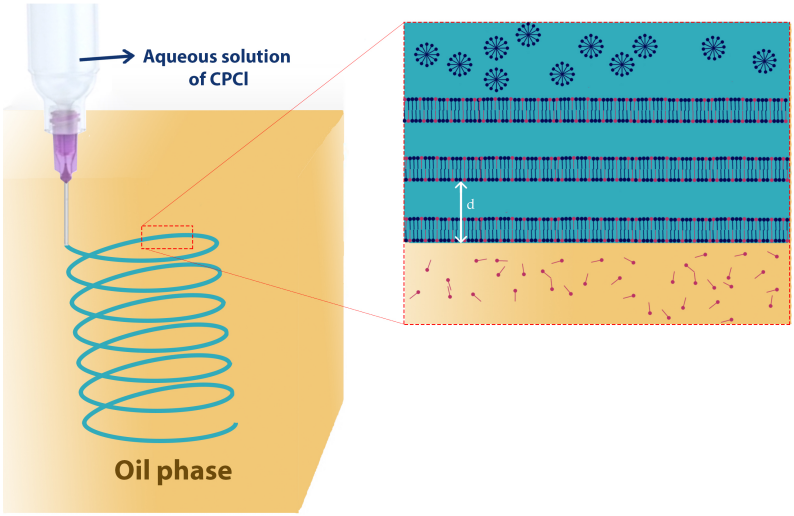

Figure 9: Schematic illustration showing the *liquid-in-liquid* 3D printing of a helical structure.

storage modulus G' than loss modulus G'', while both moduli remain insensitive to frequency (Figure 10). This rheological behavior suggests a typical solid-like viscoelastic property for the interfacial materials in agreement with the results found in previous studies [24, 43]. These results indicate that gel-like materials form at the water-oil interface during printing due to the surfactants self-assembly. In the future work, the same frequency sweep test will be carried out for the aqueous solutions of other surfactants (i.e. SDS, CTAB, and F68).

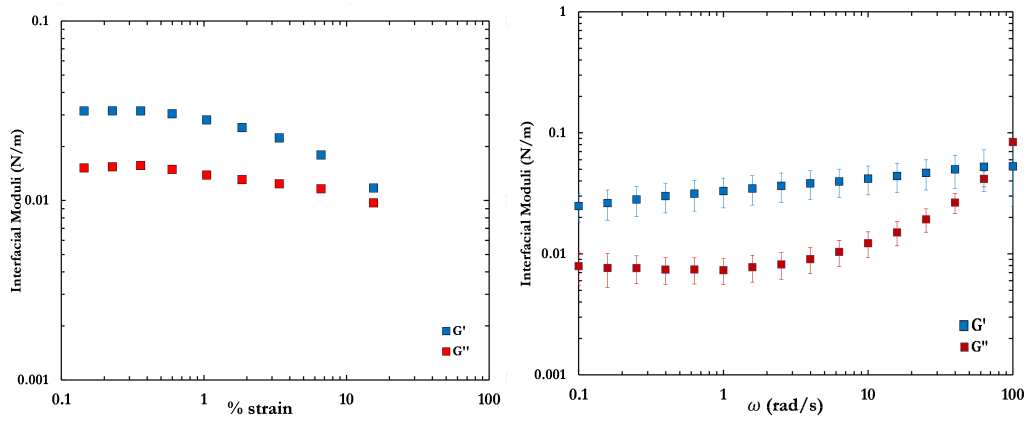

Figure 10: Interfacial rheology measurements: amplitude sweep (left) at 1 Hz and frequency sweep (right) measurements at fixed 0.1% strain and immediately after sample loading for CPCl aqueous solution (425 mM) and oil phase as shown in Figure 4.

2.4 Conclusion

In this chapter, we show the capability of surfactant self-assemblies to be used for *liquid-in-liquid* 3D printing. Different types of surfactants (ionic and nonionic) have shown to be effective in stabilizing the water-oil interface and hence, printing of liquid constructs. 2D structures once printed using ionic surfactants in aqueous solution have shown to remain stable and retain the shape for more than 4 hours. Using this approach for printing of 3D structures has proved to be promising but needs further improvement. The printing of such liquid aqueous constructs within the oil phase is enabled in this study by the self-assembly of surfactants at the water-oil interface which confines the deposited aqueous solution and maintains the dimensional stability. The printing quality in this technique is enhanced by mismatch of hydrophobicity or hydrophilicity between injected aqueous phase and the oil phase. In some *liquid-in-liquid* 3D printing methods, the miscibility between the phases is shown to limit printing precision and inhibit adhesion

between printed features [11, 14]. Interfacial rheology results for the case with CPCl as the surfactant revealed that gel-like materials form at the water-oil interface. It is hypothesized that for other types of surfactants (anionic and nonionic), the same gel-like interfacial materials form but with different moduli and robustness. Future work concerns deeper analysis and characterization of rheological properties of such interfacial materials.

CHAPTER 3

KINETIC STUDY

The self-assembly of surfactants has proved to be promising to be used in *liquid-in-liquid* 3D printing as discussed in the previous chapter. This chapter concerns the kinetic of microstructures formation at the water-oil interface during printing. Different kinetic models proposed for the interaction of surfactant systems with oil/cosurfactant are studied to determine the one that better represents the interaction between two phases involved in the printing. Since kinetic models and formation of self-assemblies at the interface, in general, is heavily dependent on the dynamics and flow characteristics of the phases, two conditions of static and dynamic are studied. In static condition, the aqueous phase is stagnant, and in dynamic condition, the aqueous solution is flowing along the oil phase. The latter model better represents the 3D printing process. This study may eventually enable us to predict and modulate the developed structures by adjusting flow characteristics as well as solution conditions (i.e. surfactant concentration).

We first discuss how the incorporation of OA molecules into CPCl micelles occurs by a process called ”solubilization”. Solubilization is the process that involves the incorporation of water-insoluble substances (oleic acid molecules in our system) into the aqueous phase of surfactant molecules (CPCl micelles) [2]. It occurs not only for small surfactant aggregates such as (nearly) spherical micelles but also for larger aggregates

including long worm-like micelles, vesicles, and lyotropic liquid crystals such as lamellar microstructures [57]. The study of solubilization of water-insoluble and hydrophobic substances and the rate at which it occurs has proven to be beneficial in various fields including but not limited to: a) physiological processes such as digestion where fatty acids are solubilized by bile salts to facilitate the absorption of fats in the gut, b) pharmaceutical industry, where drugs with limited solubility in water are dissolved by means of surfactants micelles, c) detergency including laundry and washing, and d) removal of oily soils during cleaning processes [58]. Although most studies for surfactant systems are limited to equilibrium states, the rate of solute transfer can be as important as the ultimate equilibrium solubility in the surfactant solution. Despite numerous advantages understanding thermodynamics has to offer, controlling the principles of self-assembly and establishing the decisive factors that determine final structure has yet to be addressed for many systems containing surface-active molecules [44].

For such kinetic studies, there are a variety of parameters that need to be considered, including fluid flow, surfactant concentration, and solubility limit. These factors combined together can affect the final structures through the solubilization rate of hydrophobic compounds such as oleic acid into the aqueous solution of surfactant [59, 60]. In the system studied in this work, oleic acid molecules exist as natural molecules (in the protonated state) and the effect of fatty acid dissociation appeared to be negligible at the experimental pH values according to previous studies [61]. Hence, it is hypothesized that the cosurfactancy effect of OA (rather than the electrostatic forces) causes its interaction

with CPCl aggregates. This hypothesis is supported by the previous study where the formation of the same interfacial gel-like materials was reported once oleic acid is replaced by oleylamine or oleyl alcohol [56]. The chemical structures of these oils (oleylamine and oleyl alcohol) do not allow dissociation of molecules in the aqueous solution [43].

We assume that two semi-infinite phases (aqueous and oil) are brought into contact with each other in the static condition, or the aqueous solution is flowing along the oil phase in the dynamic condition. In all estimations, both oil and aqueous phases are considered as incompressible liquids and immiscible. The thickness of the assumed water-oil interface is about $\approx$ 26 nm, equal to the highest domain spacing of lamellar structures reported previously [24]. This assumed interface contains a small layer of the oil phase and the rest is filled with the surfactant aqueous solution which either is stagnant (static) or passes along the oil phase (dynamic). For the dynamic case, it is hypothesized that the flowing aqueous solution does not cause any instabilities because of the system's hydrodynamics, so the interface will remain planar throughout the length of the assumed interface. Lastly, the system studied here is far from the equilibrium based on the solubilization rate and time scale.

There are a number of stages into the solubilization of hydrophobic substances such as fatty acid oleic acid into surfactant solutions [51, 62]. The first stage is the uptake of OA molecules by surfactant aggregates, mostly micellar aggregates. Several mechanisms in this regard can be employed to account for how surfactant aggregates absorb (uptake) oil molecules, leading to their subsequent solubilization [51]. Given the assumptions taken for each mechanism, further models can be developed to determine the

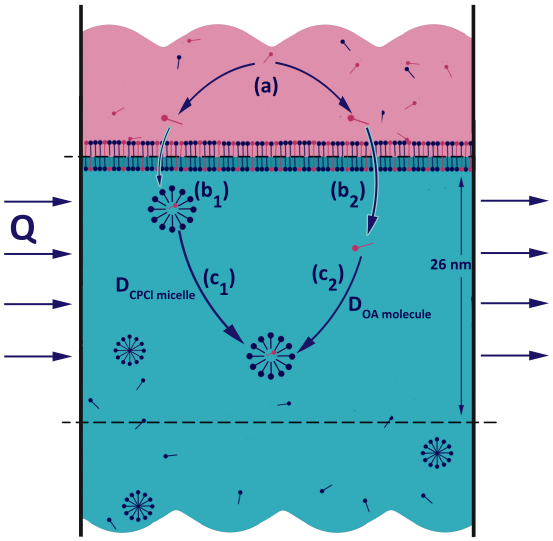

Figure 11: Schematic of two major mechanisms of solubilization of oil molecules by surfactant aggregates.

interfacial kinetics and solubilization rate.

Generally, water-insoluble solutes must first cross the water-oil interface and during this interfacial transport step, the solute molecule may undergo two distinctively different scenarios (Figure 11). It either is directly incorporated into surfactant aggregates (micelles) at the interface (mechanism 1) or enters the aqueous phase as an individual molecule (mechanism 2) [63]. We will discuss each of these mechanisms in-depth and investigate which one applies to the system in this study.

Mechanism 1: Uptake of OA molecules by surfactant aggregates (micelles) [57]

This solubilization mechanism is explained by the adsorption of surfactant aggregates. This process starts with the movement of surfactant aggregates (micelles) towards the oil phase due to the surface activity of surfactant molecules. OA molecules are then transferred into aggregates located in the immediate vicinity of the oil phase (b_1 in Figure 11)

and these oleic acid-imbibed micelles will be carried away from the oil phase either by natural or forced convection (c_1 in Figure 11). This mechanism is valid for oils with low solubility in water. Specifically, for alcohols (with C8 or longer chains) and fatty acids that have very low aqueous solubility, molecules are nearly exclusively incorporated into surfactant aggregates [64].

Mechanism 2: Solubilization of OA molecules directly into the aqueous phase as individual molecule (i.e. molecular solubilization) [51]

In this mechanism, electrostatic repulsion between surfactant aggregates prevents the close approach of micelles to the oil phase, so that solubilization results from oil molecules dissolving individually in the solution and being taken up by micelles during and/or after transport across a diffusion boundary layer to the bulk solution. That is, the solute molecule must move through the aqueous solution via convective/diffusive processes (b_2 in Figure 11). The individual solute molecules in the water phase will be eventually incorporated into the surfactant aggregates in bulk solution (c_2 in Figure 11).

It is shown that if the solubility of oil is comparable to decane, then molecular-based transport can be assumed (mechanism 2) but if it is comparable to Hexadecane which is far less soluble than decane, the other mechanism (mechanism 1) is appropriate [63]. According to earlier discussions about each mechanism and the properties of the oil in our system (oleic acid), mechanism 1 takes place for the solubilization of oleic acid molecules into the surfactant aqueous solution. In fact, it is proposed that a fatty acid like oleic acid must be able to transfer far more rapidly directly into a micelle due

to its higher surface activity and far lower molecular solubility in water [63]. Molecular simulation studies also suggest that this mechanism, i.e. the immediate exchange of OA molecules between the oil phase and the micelles holds for our system [57]. In this study, it is concluded that for long-chain molecules such as OA, solubilization induced by the adsorption of aggregates to the water-oil interface and consequent incorporation of OA molecules into these aggregates (mechanism 1) is far more significant compared to molecular dissolution of OA molecules and further uptake by micelles (mechanism 2). Worth noting that these mixed surfactant aggregates composed of surfactant and fatty acid molecules (also known as oil-imbibed micelles) exist in equilibrium with the free monomers of both oleic acid (if any) and surfactants in the surrounding aqueous phase. Some of the micelles become even larger and incorporate more surfactant molecules as they solubilize substantial amounts of OA molecules [57].

Another important aspect of this solubilization process is the location of incorporated OA molecules within the surfactant aggregates. In general, the site of solubilization within the surfactant aggregates and especially for micelles is closely related to the chemical nature of the solute. For this system and in the case of a micellar solution, oleic acid as a water-insoluble compound containing polar groups (carboxyl group) are orientated with the polar group at the core-surface interface of the micelle, and the hydrophobic group buried inside the hydrocarbon core of the micelle. Same orientation and location is favored in lamellar structure for satisfying the critical packing parameter as studied in previous work [24]. Studies have shown that this orientation is significantly affected by the partitioning coefficient of solutes between these two regions which depends strongly

on the alkyl chain length of the fatty acids.

3.1 Calculation of OA Solubilization Rate

In this section, the solubilization rate of oleic acid (OA) molecules into the aqueous solution of CPCl (within the assumed water-oil interface) is studied for different concentration of CPCl and in two conditions; 1) static (stagnant) condition where two phases have come into contact with each other suddenly, and 2) dynamic condition where the aqueous solution is flowing along the oil phase. For calculating the solubilization rate estimates at static condition, we have only the diffusion as the mechanism for the transfer of surfactant aggregates [65]. For the dynamic condition, in addition to diffusion, convective mass transfer is considered as well [62]. For both dynamic and static models, the system is considered to reach the steady-state, meaning that the assumed interface is filled with the aqueous solution of CPCl. Hence, the solubilization of OA in water is considered to be negligible while the interface is being filled.

3.1.1 Static condition (Diffusion Only - No Flow for Aqueous Phase)

For the static condition where two phases are assumed to gently come into contact with each other, the model proposed by Kabalnov et al is used [65]. In this model, the solubilization kinetics of a stagnant layer of oil in contact with the micellar solution can be calculated. That is, the rate at which oil molecules diffuse out of the oil phase and dissolve mostly into the core of surfactant micelles can be modeled based on physical parameters. The number of micelles at the interface is assumed to be constant since the concentration is significantly higher than the CMC. The assumptions in this model are as

follows:

a) No OA molecules are present in the micelles at the bulk of the aqueous solution.

b) There is no mass flux of micelles into the oil phase.

c) There is a local equilibrium between the oil monomers in water and bulk oil at the interface.

For this stagnant layer and the assumed interface, the mass flux of oleic acid molecules from the oil phase to micellar aggregates of the aqueous solution can be determined by [66]:

$$J_{oil} = \frac{D_{mic} S_{oil} n_{oil}}{tan(\kappa\sigma)}, \tag{3.1}$$

where S_{oil}, D_{mic}, and k are the molecular solubility of oleic acid in water, the diffusion coefficient of surfactant micelles in water, and reciprocal decay length of diffusion zone, respectively. S_{oil} is reported to be 0.55 mM for a saturated fatty acid with C=18 [67]. Although OA is an unsaturated fatty acid and its solubility limit is slightly higher compared to saturated fatty acid, this difference cannot be significant. This solubility limit is measured to be linearly proportional to surfactant concentration [59]. Diffusion coefficient of surfactant aggregates in water (D_{mic}) can be calculated using Stokes-Einstein equation [63, 68]:

$$D_{mic} = \frac{k_B T}{6\pi\mu R_0}, \tag{3.2}$$

where μ, R_0, k_B, and T are viscosity of the aqueous phase, radius of surfactant micelles,

Boltzman's constant, and temperature, respectively. The value of diffusion coefficient is calculated based on the radius of micelles which itself is dependent on surfactant concentration (C).

k in Equation 3.1 is defined as reciprocal decay length of diffusion zone. This parameter (k) can be calculated for the case of an oil (i.e. oleic acid) in a surfactant aqueous solution based on the following formula [65]:

$$k^2 = \frac{k_+ n_{mic}}{D_{oil}}, \tag{3.3}$$

where k_+ is the association constant of an oleic acid molecule with micelles, and n_{mic} is the concentration of micelles at the assumed interface, determined by surfactant concentration (C). The following equation gives a rough, but reasonable estimate of the association rate constant (k_+) [65]:

$$k_+ = 4\pi D_{oil} R_0, \tag{3.4}$$

where D_{oil} is the diffusion coefficient of oleic acid molecules in water.

Based on the Equation 3.1, the mass flux of OA into the aqueous phase with different concentrations of CPCl are calculated and provided in Table 4. Number of micelles in the assumed interface is also calculated and the radii of micelles are obtained from the work of Niroobakhsh et al. [56].

Table 4: Mass flux of OA into different concentration of aqueous CPCl solution under static condition (i.e. no flow)

Concentration mM	**Radius of micelles [56]** nm	**Concentration of micelles** micelles/m^3	**Mass flux of OA** kg/cm^2.s
50	2.12	5.58E+23	3.35E-12
190	2.2	2.12E+24	6.7E-12
425	2.4	4.74E+24	1.05E-11

3.1.2 Dynamics Condition (Convective Mass Transfer - Flowing Aqueous Solution)

Huang et al. for the first time calculated the convective mass transfer for a spinning liquid disc for linoleic acid (a fatty acid) in aqueous solutions of sodium taurodeoxycholate (ionic surfactant) and provided a powerful method for liquid-liquid mass transfer in the presence of flow [62]. In fact, they extended the convectional study of solid dissolution to the solubilization of liquids in another liquid by focusing on the physical process of mass transfer and fluid flow. Since the flow rate next to the interface is fast, the kinetics is not diffusion-controlled as opposed to the static condition discussed earlier [62]. In this model, the mass transfer is dominated by external convection which is the rotation of the disk. The same approach can be employed for our system where an aqueous solution of surfactant is flowing along the oil phase (external forced convection flow) [69]. In this approach, we can use the following equation for driving the mass flux of OA into the aqueous phase [69]:

$$Sh_x = 0.664 Re_x^{1/2} S_c^{1/3}, \tag{3.5}$$

where Sh_x, S_c, and Re_x are the dimensionless numbers, Sherwood, Schmidt, and Reynolds, respectively. These numbers can be calculated from the following equations [69]:

$$Sh_x = \frac{k_c L}{D_{mic}}, \tag{3.6}$$

$$S_c = \frac{\mu}{\rho D}, \tag{3.7}$$

$$Re_x = \frac{\rho u L}{\mu}, \tag{3.8}$$

where L the characteristic length which is the length of the assumed interface in this case. K_c is the mass transfer coefficient that will be used for the calculation of the solubilization rate. For calculation of Schmidt number, the viscosity and density (μ and ρ) of the aqueous solution of CPCl were used. For this equation, the diffusion coefficient of surfactant micelles (D_{mic}) was used instead of OA diffusion coefficient since surfactant aggregates carry OA molecules into the bulk of the aqueous phase as discussed earlier in this chapter (mechanism 1). Based on the Equation 3.5, the flow rate and surfactant concentration of the aqueous phase manifest their effect on the solubilization rate through Reynolds number and Schmidt number, respectively. Given the mass transfer coefficient calculated earlier from Sherwood number Sh_x, the mass flux of oleic acid (mole of OA over the unit of area and time, N_{OA}) into the aqueous phase under physical dissolution conditions in the presence of surfactants can be estimated by solving the following equation [69]:

$$N_{OA} = k_c(C_{oil\ phase} - C_{aqueous\ phase}), \tag{3.9}$$

where $C_{oil\ phase}$ is the equilibrium concentration of oleic acid in the bulk phase of oil, $C_{Aqueous\ phase}$ is its concentration in the aqueous solution at any time, and N_{OA} is the mass flux of OA into the aqueous phase in unit of mole/m^2.s. Oleic acid concentration in the aqueous solution is hypothesized to be zero ($C_{Aqueous\ phase}$=0) before contact and the oleic acid concentration was reported by the manufacturer to be $C_{oil\ phase}$ = 3.15 M. The concentration of oleic acid in the oil phase scarcely changes during the transport since the volume is relatively large. Then, mass fluxes as a function of both flow rate (Q) and surfactant concentration (C) are calculated and provided in Tables 5 and 6.

Table 5: Mass flux of OA into aqueous phase with constant concentration (C=100 mM) at different flow rates under dynamic condition (i.e. flowing aqueous solution)

Flow rate, Q ml/h	Reynolds, Re	Schmidt, S_c	Sherwood, Sh_x	Mass transfer coefficient, k_c m/s	Mass flux of OA kg/cm^2.s
1	0.7	3017	7.7	5.69E-06	5.08E-07
300	139	3017	109	8.00E-05	7.16E-06
400	186.45	3017	126	9.28E-05	8.3E-06

Table 6: Mass flux of OA into aqueous phase with constant flow rate (C=100 ml/h) at different surfactant concentrations under dynamic condition (i.e. flowing aqueous solution)

Concentration, C mM	Reynolds, Re	Schmidt, S_c	Sherwood, Sh_x	Mass transfer coefficient, k_c m/s	Mass flux of OA kg/cm^2.s
50	46.6	3.8E+03	63	4.67E-05	4.18E-06
190	46.6	3.8E+03	70	5.170E-05	4.62E-06
425	46.6	3.8E+03	87	6.41E-05	5.73E-06

We used Fick's law of diffusion to study how aggregates tend to spread from a

region of higher concentration to a region of lower concentration and is expressed as $\sigma = (2D_{mic}t)^{1/2}$ (where σ, D_{mic}, and t are the diffusion length, diffusion coefficient of CPCl micelles under random thermal motion, and time, respectively) [69]. Using this correlation and given the fact that OA molecules are carried by CPCl micelles, the diffusion length at different time scales can be estimated. We consider a given contacting area between the aqueous phase and the oil phase and then convert these mass fluxes to mass rates. The mass rates of OA into the aqueous phase for both dynamic and static conditions are plotted over time (Figure 12). In the static case, the mass rate becomes constant at the time scale of microseconds. Using Fick's law, this time scale corresponds to a diffusion length of 26 nm. The mass rate follows the same trend for all CPCl concentrations. In contrast, for the dynamic condition, the mass rate of OA proved to be constant over time. It is evident that in dynamic condition with the presence of force convection (flowing aqueous solution), the mass flux of OA (hence the mass rate of OA into the aqueous phase) is significantly higher (five orders of magnitude) than that of the static case, similar to other work [57]. With the measured estimates for OA solubilization rates in two static and dynamic condition, the composition of the water-oil interface at each time scale can be obtained and based on an established ternary phase diagram, the formed structures can be predicted during the nonequilibrium printing condition.

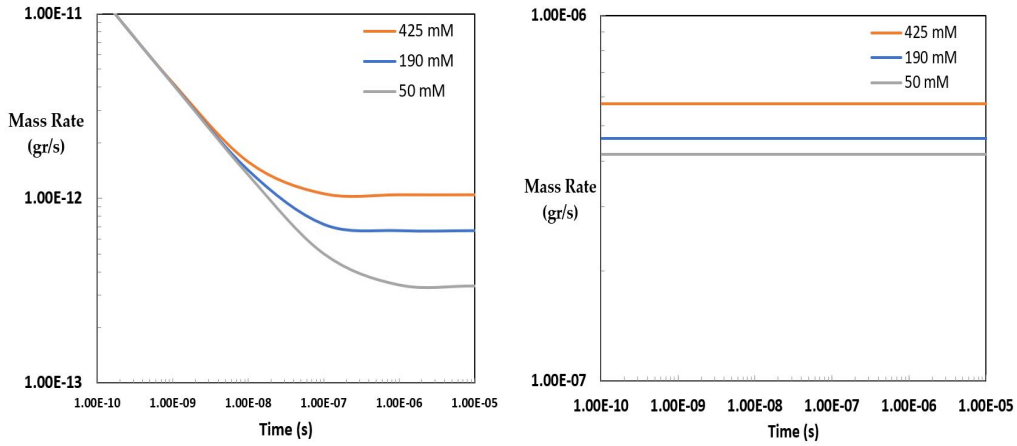

Figure 12: Mass rates of OA into surfactant aqueous solutions over time for different concentration of CPCl in both static (left) and dynamic (right) conditions. The flow rate of aqueous solution in dynamic condition is Q= 100 ml/h.

3.2 Conclusion

In this chapter, kinetic aspects of surfactant self-assembly formation at the interface are investigated. For the static and dynamic conditions, two kinetic modelings are established and used to estimate the solubilization rate of OA into the aqueous solution of surfactant. Using these models, one can derive the rate of self-assembly formation in nonequilibrium conditions (such as printing), and hence control the physical and mechanical properties of the interfacial materials. This opportunity in turn enables us to further improve the printing quality by tuning the viscoelastic properties of interfacial materials. Additionally, by changing the aqueous phase conditions such as surfactant concentration and flow rate, we can theoretically predict the preferred morphology using an established ternary phase diagram of the system (water/oil/surfactant).

CHAPTER 4

COMPUTATIONAL SIMULATION (DISSIPATIVE PARTICLE DYNAMICS)

Experimental setups have shown to be limited in providing insight into complex interactions at the molecular level within such complex systems. Computer simulations, however, have been used as powerful tools for the investigation of dynamics at the microscopic scale [70, 71]. In many computer simulations, time and length scales are limiting factors. As an alternative method, mesoscopic simulations such as dissipative particle dynamics (DPD) are used to investigate the mesostructure of systems up to the microsecond range [72]. Dissipative Particle Dynamics (DPD) is a stochastic simulation technique to investigate different stages of microstructure formation while providing insight into the dynamics of the system [55, 71, 73]. In this technique, the simulation strategy is to group atoms together into single "beads" and use these centers of mass as new simulation entities. Then interactions between these beads which are represented by DPD conservative interaction parameters occur at the mesoscopic levels. These conservative interaction parameters represent van der waals, electrostatic, hydrophobicity, and hydrogen bonding [72].

There have been some studies on DPD simulation of ternary phases composed of water/surfactant/oil [74], but limited studies are available where the oil is polar and has surface activity. For this work, the DPD simulation technique is employed to study the formation of the microstructures at an interface when two components (i.e. surfactant

and polar oil) interact with each other. Toward this goal, we determine the simulation parameterization as well as representation of two components used in the printing (CPCl and OA) based on their experimental behaviors once dissolved in water separately. The resulting structures in the simulations (i.e. spherical micelles, cylindrical micelles, vesicles, and lamellar) are evaluated by previously reported studies in which methods such as small-angle X-ray scattering (SAXS) measurements, visual inspection, or other computer simulations techniques were used [56, 75]. We keep adjusting the interaction parameters and molecular representation for each component until an acceptable behavior is observed in simulation with respect to experiments. Then all three components (CPCl, OA, and water) with adjusted interaction parameters will be mixed together and interact with one another within a simulation box which represents the water-oil interface (with a thickness of $\approx$ 35 nm). Evolution of the system to different microstructures and underlying mechanisms is then studied and the way a surfactant/water system reacts to the introduction of a polar oil is understood.

4.1 DPD Parameterization

For this computational study, open source polymer research engine - dissipative particle dynamics (Osprey-DPD) has been utilized which can be found on Github [76]. The first step is to correlate conservative interaction parameters of DPD with the behaviors of both pure surfactant (CPCl) in water and oleic acid in water systems so that they better represent themselves in the simulations. First, we select the initial conservative parameters based on the chemistry of components and previous studies of amphiphilic

molecules in water [50, 77]. Then we adjust conservative interaction parameters directly and based on experimental results for each component. In the simulations, each molecule is represented with certain beads. All length scales are measured in units of the bead diameter (r_0) and all forces in units of $\frac{k_B T}{r_0}$ (where k_B and T are Boltzmann constant and temperature, respectively). Dimensions of the box in all the simulations are L_x= $32r_0$ $\times$L$_y$= $32r_0$ $\times$L$_z$= $32r_0$. If we choose the bead density equal to ρr_0^3=3, the simulation box contains 98304 beads and periodic boundary conditions were applied in all three directions. The simulation runs for 2,000,000 steps with a time step of 0.05 (dimensionless). Both the temperature and the hydrostatic pressure are checked at the end to assure that system has reached an equilibrium. The structure of the system is determined by visual inspection after equilibrium was reached.

The DPD particles or beads represent small volumes of fluid rather than single atoms so that their interactions are softly repulsive and short-ranged [73]. All interaction potentials have the same range r_0, but their amplitudes a_{ij} differ for different bead species. Amphiphilic molecules such as CPCl and oleic acid have been modeled in many DPD studies as dimers composed of a hydrophilic head and a hydrophobic tail [77], but there have been limited studies in which surfactants are truly represented based on their molecular structures [50]. The systems studied here are built up from six bead species: M and N (collectively represent CPCl head group), H (OA head group), C and C$_1$ (hydrocarbon chains), and W (for water). Here we represent the surfactant molecule as well as oleic acid each with 7 beads as shown in Figure 13. The architecture of both CPCl and OA lipid molecules is constructed by connecting adjacent beads with Hookean spring potentials.

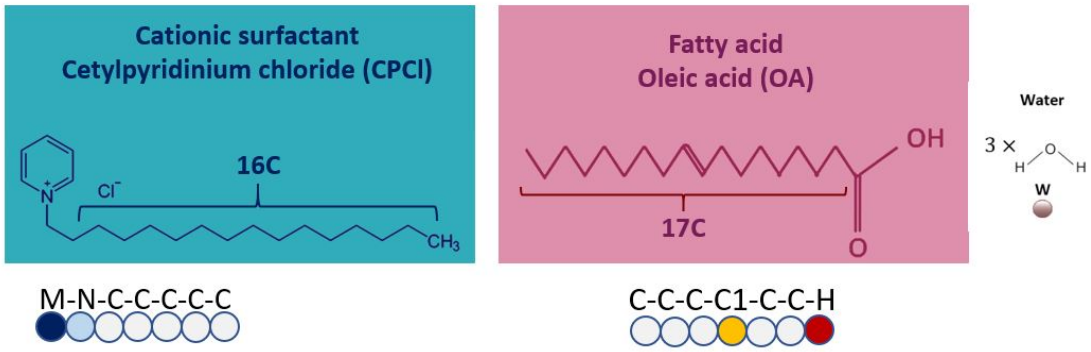

Figure 13: Representations of molecules (head group of CPCl represented with two beads: N & M, N representing the hydrophilic, and M the charged section and bulky nature of the surfactant).

All beads have the same mass, m_0. The Hookean bonds and chain stiffness parameters are identified by the names of the beads defining them. Hence, CPCl as an example with MNC_5 structure requires three bond types, MN, NC, and CC, and allows three possible chain stiffness potentials, MNC, NCC, and CCC. The dissipative force parameters are 4.5 for all bead pairs (in units of $\sqrt{(m_0 k_B T/r_0^2)}$). The same value of 128 (in units of $k_B T/r_0^2$) is used for all bonded beads. Chain stiffness is imposed by a bending potential for all sets of three bonds along the backbone with bending constant of 15.

For determining the interaction between different types of beads, the overlap and interaction strength of the water beads is used here to reproduce the water compressibility and density fluctuations of water [73]. The remaining force amplitudes (a_{ij}) will be fine-tuned to match the properties of their corresponding self-assembly behavior, by carefully determining the effects of changes to each parameter on the self-assembly behavior.

4.2 CPCl Phase Behavior in Water

The head group of CPCl is represented with two bead types, N & M. M type bead represents the charged behavior and bulky nature of the pyridinium head group while N type bead correlates with the hydrophilicity of the head group. As expected from experimental results, for a certain range of surfactant concentration, the amphiphiles aggregate into well-ordered structures because of the strong repulsion between the chain beads and the solvent beads, mimicking the hydrophobic effect for hydrocarbon chains in water. Critical Packing parameter has been discussed already in Introduction Chapter and we will use it here to account for the preferred structures for the molecules. In general, at CPPl$\leq$1/3, the molecules self-assemble into spherical micelles while for higher concentrations, the micelle becomes nonspherical (ellipsoidal), until they transform into cylindrical or rod-like micelle around CPP $\approx$1/2 [1]. CPCl molecule has a bulky charged head group and one hydrocarbon tail. Hence, for CPCl, we can imagine that CPP lies roughly between 1/3 to 1/2 for the concentration range we will simulate in this study (50 - 425 mM). The experimental result for CPCl specifically suggests the formation of prolate ellipsoidal micelles which encompass both rod-like and spherical micelles at 100 mM while at 400 mM, oblate ellipsoidal (disk-like) micelles appear based on SANS data [24,75,78]. In this context, a prolate (elongated) spheroid results if an ellipse is rotated about its major axis, shaped like an American football. If the ellipse is rotated about its minor axis, the result is an oblate (flattened) spheroid. The self-assembly behavior of CPCl as mentioned earlier is most likely due to the fact that once the CPCl micelle becomes larger and the aggregation number increases, the crowding of hydrocarbon chains at the center of

the micelle decreases the configurational entropy of the chains. This decrease in entropy results in formation of an oblate (ellipsoidal) structure to accommodate more surfactant molecules in the micelles [1, 78]. In addition, due to the bulkiness of the pyridinium head group for CPCl surfactant, a more flat surface is more favorable as this structure accommodates larger number of CPCl molecules.

Based on these discussions, the conservative interaction parameters for CPCl beads (M, N, C) are adjusted accordingly to achieve such self-assembly behavior. These interaction values are reported in Table 7. It worth noting that all beads in DPD simulation are repulsive to each other and these values only determine the extent to which different type of beads are repulsive to one another. Although the DPD simulations do not have charges per se, we are representing its effect by making beads more strongly repelled from each other through conservative interaction parameters. Therefore, the interaction parameter between M beads is made highly repulsive (a_{MM}=50) because the pyrindium head group (a benzen ring with charged interaction) is bulky. The phase behavior of CPCl according to interaction parameters in Table 7 is shown in Figure 14. These snapshots demonstrate the structures that form in DPD simulation at different concentrations of CPCl solutions. The oblate ellipsoidal (disk-like) micelles observed in these simulations are consistent with the SAXS data of pure CPCl micelles in terms of the length distribution [78].

Table 7: DPD conservative interactions for beads of CPCl and water

	W	N	M	C
W	25	25	25	80
N	25	25	25	80
M	25	25	50	80
C	80	80	80	25

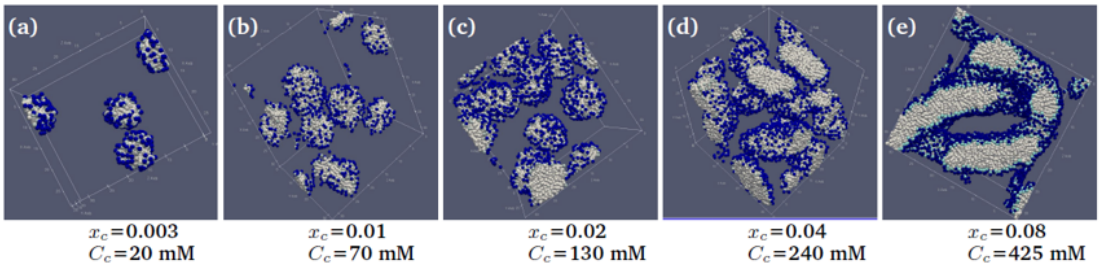

Figure 14: CPCl self-assembly behavior in simulation based on conservative interactions reported in Table 7.

4.3 OA Phase Behavior in Water

Oleic acid (OA) has n = 18 carbons in the hydrocarbon chain with a cis-double bond, which makes the chain length shorter than a saturated chain. For example, for a saturated hydrocarbon chain with n carbon atoms, l_c and v can be written as follows according to [79].

$$l_c \leq (0.154 + 0.1265n)\, nm, \tag{4.1}$$

$$v \approx (27.4 + 26.9n) \times 10^{-3} nm^3, \tag{4.2}$$

For a saturated hydrocarbon chain with n = 18 the chain length is about $l_c \approx 2.43$ nm from Equation 4.1, but we can roughly consider the l_c for OA equals to the CPCl chain length with n = 16 (l_c = 2.2 nm). OA has surface activity due to its polar carboxyl head group, giving rise to the cosurfactancy effect [80].

Janke et al. studied the molecular dynamics of oleic acid in water as a function of protonation of the head group (hence pH) and concentration. As discussed in Chapter 3, in

the experimental conditions with a pH of around 7, it is expected that the majority of OA molecules remains protonated and neutral [61, 81]. Hence, by dissolving OA into water, we expect to have what was defined as the ”oil phase” rather than micelles or vesicles in this condition [61]. The oil phase is in fact formed as the spherical aggregates (such as small oil droplets) with monomer head groups packed on the surface, but lack a single aqueous interior and a bilayer structure [61].

In order to have the described phase of OA in water, we modified the conservative interaction parameters. These adjusted parameters are provided in Table 8. The resulting morphologies for the OA in the DPD simulation at different concentrations are shown in Figure 15, in agreement with the results of Janke et al [61]. The structure obtained here is the same ”oil phase” with spherical morphology, but with small aqueous interior. This block of water that we observe at the center of aggregates is not against our expectation, given the variation in experimental conditions such as pH and temperature, which may result in a low degree of dissociation for OA molecules.

Table 8: DPD conservative interactions for beads of OA and water

	W	H	C1	C
W	25	20	25	80
H	20	15	25	50
C1	80	50	25	25
C	80	80	25	25

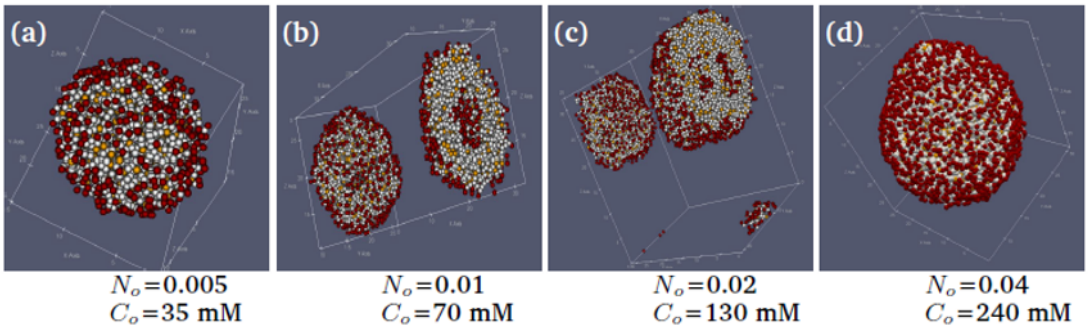

Figure 15: OA phase behavior in water in different concentrations.

4.4 Ternary Phase Behavior

The self-assembly and phase behavior of OA and CPCl have been reproduced with DPD. The results are in agreement with experiments and the conservative parameters are consistent with other work on DPD simulation of amphiphiles [82]. In final step, the phase behavior of the ternary mixtures of water/OA/CPCl will be studied at the same determined parameterization. All interactions between beads are listed in Table 9. The only interaction which needs to be found prior to simulation of the ternary phase is the interaction between head groups of OA and CPCl, i.e. a_{MH} and a_{NH} (illustrated as χ in Table 9). Hence, the simulations are performed in three scenarios to investigate the effect of these interaction parameters on the resulting structure. In these scenarios, this interaction is varied from being less repulsive (a_{MH}=a_{NH}=15) to higher repulsion (a_{MH}=a_{NH}=25) and to highest repulsion (a_{MH}=a_{NH}=50). The phase behavior of the system for three scenarios are provided in Figure 16.

The comparison of formed structure in these scenarios indicates that the interaction between the head group of CPCl and OA (χ) does not have any significant effect on

Table 9: DPD conservative interactions of all beads. χ denotes interaction between head groups of OA and CPCl.

	W	N	M	H	C	C1
W	25	25	25	20	80	80
N	25	25	25	χ	80	80
M	25	25	50	χ	80	80
H	25	χ	χ	15	50	50
C	80	80	80	50	25	25
C1	80	80	80	50	25	25

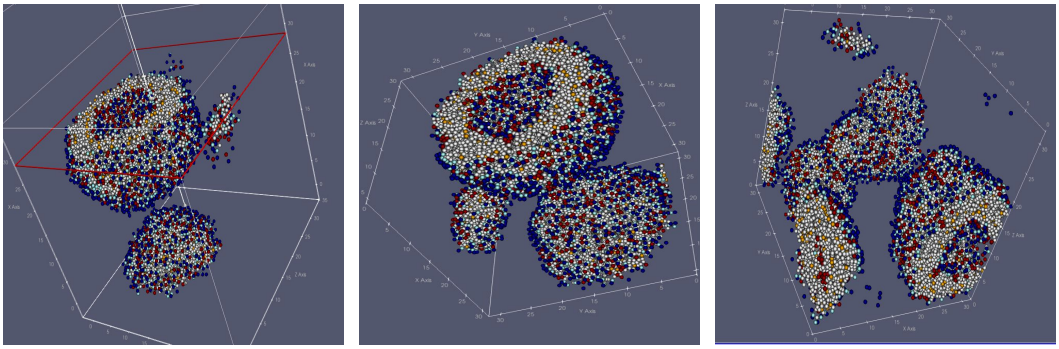

Figure 16: Phase behavior of the ternary system for three scenarios with respect to interaction between CPCl and OA head groups (a_{MH} and a_{NH}). From left to right, the head groups of CPCl and OA are $\chi = 15$, $\chi = 25$, and $\chi = 50$.

the resulting morphology. The only observable difference is the number of aggregates in the case of $\chi = 50$ which is increased to more than one aggregates (i.e. one unilamellar vesicle and two micelles). However, the interaction of $\chi = 25$ (second scenario) between head groups seems to be a better approximation of the real system based on the physicochemistry of molecules. Therefore, the evolution of the structure for this scenario over time is simulated and shown in Figure 17. Once the simulation starts, all the molecules are randomly dispersed within the simulation box. Over time, the components assemble into a vesicle. These snapshots of the simulated system show the morphological pathway for a vesicle which is otherwise impossible to achieve from experimental studies. Having a computation simulation tool such as DPD which is validated by experimental results will allow us to investigate the structures that form at the water-oil interface during printing. Hence, we may be able to computationally investigate whether the formed structures can be fine tuned by selection of aqueous phase components.

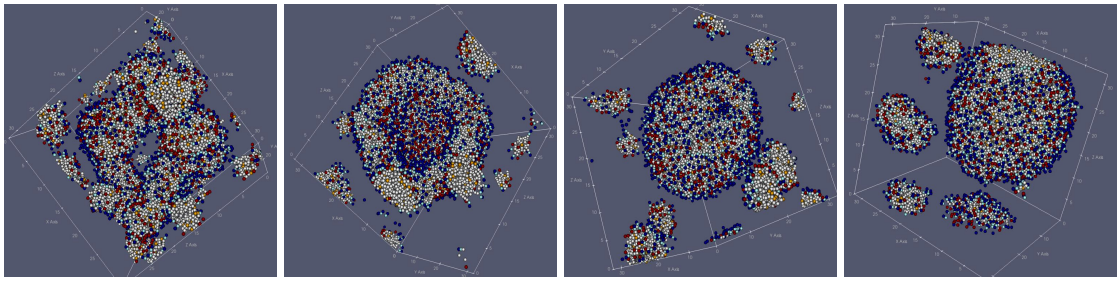

Figure 17: Self-assembly behavior and structure evolution of ternary system (with an equimolar mixing ratio of CPCl and OA) for the case with χ=25.

4.5 Conclusion

In this chapter, the self-assembly behavior of oleic acid in water and CPCl surfactants in water are reproduced successfully and validated by experimental results. A reliable parameterization and topology for each molecule are then obtained which can be used to investigate details in molecular scale for each component and at different concentrations. Then, the structure of the ternary phase at an equimolar mixing ratio of CPCl and OA is simulated and the effect of interaction between head groups of surfactant and oil is discussed. The evolution of a ternary system to a vesicle is also demonstrated and the morphological pathway is discussed. For the future work, the system size dependence on the consistency of results will be studied to investigate whether formation of any structure is affected by simulation size box.

CHAPTER 5

CONCLUSION AND FUTURE WORK

5.1 Conclusion

In this study, a novel *liquid-in-liquid* 3D printing is introduced which allows for patterning the low-viscous aqueous solution of surfactants into predefined structures within an oil phase. Spontaneous self-assembly of surfactants at the water-oil interface enables printing of such constructs and proved to be applicable to all types of surfactants (cationic, anionic, and non-ionic). Printing of such soft materials as aqueous solutions has previously not been possible with neither traditional *layer-by-layer* 3D printing nor with current *liquid-in-liquid* 3D printing approaches. In fact, the designs which are printed here (i.e. 2D planar meandering channel and a 3D helical structure with overhanging features) are complex enough to suggest the capability of our method to extend the potential of *liquid-in-liquid* 3D printing and to be used for soft materials such as aqueous solutions. The reported printing technique here does not require any rheological properties for the printing phase and the support oil phase, in contrast to other *liquid-in-liquid* 3D printing methods. The aqueous solution as the dispensed phase can be easily formulated with different classes of material such as bioinks (for tissue engineering) which are mostly polymer-based aqueous solutions loaded with cells. In this research, we have also investigated the influence of kinetic factors on structural assembly and regulation of the resultant

microstructures based on both types of building blocks and dynamic conditions. Dynamics, kinetics, and mechanisms of oil solubilization in the aqueous phase are discussed as the key factor for the formation of nanostructure at the interface. Interaction between constituent components is elaborated and relevant kinetic modelings are established which in turn allows for qualitative understanding of the dynamics behind the formation of such self-assemblies at the water-oil interface. In dissipative particle dynamics study, the self-assembly behavior of two phases involved in 3D printing is reproduced successfully based on their experimental results. The computational study on thermodynamics of our system demonstrates how microstructures at the water-oil interface evolve and further interpretation provides insight into dynamics and the underlying morphological pathway for the microstructure formation. The models established in kinetic study along with computational simulation tool (DPD) allow us to predict formation of structures at the water-oil interface and to tailor desired microstructured materials and their properties. These capabilities can be further used in the reported *liquid-in-liquid* 3D printing to fine tune the internal structures of prints in nano- or microscale in order to impart functionality.

5.2 Future Work

The printed constructs in this printing approach are believed to be dynamic meaning that they can be adjusted and altered by their external environment, which can create a new possibility to print biomimetic, and responsive materials. Furthermore, the stability of printed structures can be enhanced with different methods such as the addition of a photocurable polymer to the printing aqueous solution and subsequent crosslinking

of printed constructs. Upon successful implementation, our *liquid-in-liquid* 3D printing method could pave the way for the application of surfactant self-assembly in the fabrication of robust constructs with internal nanostructures and spatially defined features. Such capability can be used in regenerative medicines by providing a platform to print self-assembling biomaterials into complex tissue mimics where internal supramolecular structures and their functionality control biological processes, similar to the natural extracellular matrix. Using kinetic study and established modelings, we will be able to control the physical and mechanical properties of the interfacial materials by changing the aqueous phase conditions such as surfactant concentration and flow rate. This opportunity in turn enables us to further improve the printing quality by tuning the viscoelastic properties of interfacial materials. Computational simulation shows the successful reproduction of the self-assembly behavior of two phases and can be applicable to any type of surfactant system. Future computational work will be focused on how molecular structures and interaction of components would eventually affect the resulting morphology. We can computationally investigate the possibility to tune the microstructure formation through careful selection of constituent components (aqueous and oil phases), which can be of use in applications where specific hierarchical ordering in nano- or microscale is required.

REFERENCE LIST

[1] J. N. Israelachvili, *Intermolecular and surface forces*. Academic press, 2011.

[2] A. T. Florence and D. Attwood, *Physicochemical principles of pharmacy: In manufacture, formulation and clinical use*. Pharmaceutical press, 2015.

[3] M. J. Rosen and J. T. Kunjappu, *Surfactants and interfacial phenomena*. John Wiley & Sons, 2012.

[4] A. Bandyopadhyay, S. Bose, and S. Das, "3d printing of biomaterials," *MRS Bulletin*, vol. 40, no. 2, pp. 108–115, 2015.

[5] H. N. Chia and B. M. Wu, "Recent advances in 3d printing of biomaterials," *Journal of Biological Engineering*, vol. 9, no. 1, pp. 1–14, 2015.

[6] G. Luo, Y. Yu, Y. Yuan, X. Chen, Z. Liu, and T. Kong, "Freeform, reconfigurable embedded printing of all-aqueous 3d architectures," *Advanced Materials*, vol. 31, no. 49, p. 1904631, 2019.

[7] S. Chen, W. S. Tan, M. A. B. Juhari, Q. Shi, X. S. Cheng, W. L. Chan, and J. Song, "Freeform 3d printing of soft matters: recent advances in technology for biomedical engineering," *Biomedical Engineering Letters*, pp. 1–27, 2020.

[8] C. S. OâBryan, T. Bhattacharjee, S. Hart, C. P. Kabb, K. D. Schulze, I. Chilakala, B. S. Sumerlin, W. G. Sawyer, and T. E. Angelini, "Self-assembled microorganogels for 3d printing silicone structures," *Science Advances*, vol. 3, no. 5, p. e1602800, 2017.

[9] S.-W. Hu, P.-J. Sung, T. P. Nguyen, Y.-J. Sheng, and H.-K. Tsao, "Uv-resistant self-healing emulsion glass as a new liquid-like solid material for 3d printing," *ACS Applied Materials & Interfaces*, vol. 12, no. 21, pp. 24 450–24 457, 2020.

[10] L. Shi, H. Carstensen, K. HoÌlzl, M. Lunzer, H. Li, J. Hilborn, A. Ovsianikov, and D. A. Ossipov, "Dynamic coordination chemistry enables free directional printing of biopolymer hydrogel," *Chemistry of Materials*, vol. 29, no. 14, pp. 5816–5823, 2017.

[11] T. J. Hinton, A. Hudson, K. Pusch, A. Lee, and A. W. Feinberg, "3d printing pdms elastomer in a hydrophilic support bath via freeform reversible embedding," *ACS Biomaterials Science & Engineering*, vol. 2, no. 10, pp. 1781–1786, 2016.

[12] T. Bhattacharjee, S. M. Zehnder, K. G. Rowe, S. Jain, R. M. Nixon, W. G. Sawyer, and T. E. Angelini, "Writing in the granular gel medium," *Science Advances*, vol. 1, no. 8, p. e1500655, 2015.

[13] N. Noor, A. Shapira, R. Edri, I. Gal, L. Wertheim, and T. Dvir, "3d printing of personalized thick and perfusable cardiac patches and hearts," *Advanced Science*, vol. 6, no. 11, p. 1900344, 2019.

[14] J. Forth, X. Liu, J. Hasnain, A. Toor, K. Miszta, S. Shi, P. L. Geissler, T. Emrick, B. A. Helms, and T. P. Russell, "Reconfigurable printed liquids," *Advanced Materials*, vol. 30, no. 16, p. 1707603, 2018.

[15] G. Villar, A. D. Graham, and H. Bayley, "A tissue-like printed material," *Science*, vol. 340, no. 6128, pp. 48–52, 2013.

[16] A. D. Graham, S. N. Olof, M. J. Burke, J. P. Armstrong, E. A. Mikhailova, J. G. Nicholson, S. J. Box, F. G. Szele, A. W. Perriman, and H. Bayley, "High-resolution patterned cellular constructs by droplet-based 3d printing," *Scientific Reports*, vol. 7, no. 1, pp. 1–11, 2017.

[17] T. Maruyama, H. Matsushita, J.-i. Uchida, F. Kubota, N. Kamiya, and M. Goto, "Liquid membrane operations in a microfluidic device for selective separation of metal ions," *Analytical Chemistry*, vol. 76, no. 15, pp. 4495–4500, 2004.

[18] T. Leistner, M. Türk, A. Weber, C. Weber, and U. A. Peuker, "Selective separation using fluid-liquid interfaces," in *Materials Science Forum*, vol. 959. Trans Tech Publ, 2019, pp. 113–124.

[19] S. Berg, "Marangoni-driven spreading along liquid-liquid interfaces," *Physics of Fluids*, vol. 21, no. 3, p. 032105, 2009.

[20] B. Qiao, J. V. Muntean, M. Olvera de la Cruz, and R. J. Ellis, "Ion transport mechanisms in liquid–liquid interface," *Langmuir*, vol. 33, no. 24, pp. 6135–6142, 2017.

[21] K. Miyazawa, J.-i. Minato, T. Yoshii, M. Fujino, and T. Suga, "Structural characterization of the fullerene nanotubes prepared by the liquid–liquid interfacial precipitation method," *Journal of Materials Research*, vol. 20, no. 3, pp. 688–695, 2005.

[22] F. Bresme and M. Oettel, "Nanoparticles at fluid interfaces," *Journal of Physics: Condensed Matter*, vol. 19, no. 41, p. 413101, 2007.

[23] K. r. Larsson, "Stability of emulsions formed by polar lipids," *Progress in the Chemistry of Fats and Other Lipids*, 1978.

[24] Z. Niroobakhsh, J. A. LaNasa, A. Belmonte, and R. J. Hickey, "Rapid stabilization of immiscible fluids using nanostructured interfaces via surfactant association," *Physical Review Letters*, vol. 122, no. 17, p. 178003, 2019.

[25] J. Gargiuli, E. Shapiro, H. Gulhane, G. Nair, D. Drikakis, and P. Vadgama, "Microfluidic systems for in situ formation of nylon 6, 6 membranes," *Journal of Membrane Science*, vol. 282, no. 1-2, pp. 257–265, 2006.

[26] G. Nair, J. F. Gargiuli, N. R. Shiju, Z. Rong, E. Shapiro, D. Drikakis, and P. Vadgama, "In situ fabrication of cross-linked protein membranes by using microfluidics," *ChemBioChem*, vol. 7, no. 11, pp. 1683–1689, 2006.

[27] M. F. Jimenez-Solomon, Q. Song, K. E. Jelfs, M. Munoz-Ibanez, and A. G. Livingston, "Polymer nanofilms with enhanced microporosity by interfacial polymerization," *Nature Materials*, vol. 15, no. 7, pp. 760–767, 2016.

[28] J.-A. Yang, J. Yeom, B. W. Hwang, A. S. Hoffman, and S. K. Hahn, "In situ-forming injectable hydrogels for regenerative medicine," *Progress in Polymer Science*, vol. 39, no. 12, pp. 1973–1986, 2014.

[29] T. Jungst, W. Smolan, K. Schacht, T. Scheibel, and J. Groll, "Strategies and molecular design criteria for 3d printable hydrogels," *Chemical Reviews*, vol. 116, no. 3, pp. 1496–1539, 2016.

[30] K. Piradashvili, E. M. Alexandrino, F. R. Wurm, and K. Landfester, "Reactions and polymerizations at the liquid–liquid interface," *Chemical Reviews*, vol. 116, no. 4, pp. 2141–2169, 2016.

[31] A. Mendoza-Meinhardt, L. Botto, and A. Mata, "A fluidic device for the controlled formation and real-time monitoring of soft membranes self-assembled at liquid interfaces," *Scientific Reports*, vol. 8, no. 1, pp. 1–9, 2018.

[32] R. M. Capito, H. S. Azevedo, Y. S. Velichko, A. Mata, and S. I. Stupp, "Self-assembly of large and small molecules into hierarchically ordered sacs and membranes," *Science*, vol. 319, no. 5871, pp. 1812–1816, 2008.

[33] J. J. Cardiel, D. Takagi, H.-F. Tsai, and A. Q. Shen, "Formation and flow behavior of micellar membranes in a t-shaped microchannel," *Soft Matter*, vol. 12, no. 39, pp. 8226–8234, 2016.

[34] N. Jia, E. Rosella, E. Juère, R. Pouliot, F. Kleitz, and J. Greener, "A microfluidic approach to micromembrane synthesis for complex release profiles of nanocarriers," *Lab on a Chip*, vol. 20, no. 6, pp. 1066–1071, 2020.

[35] S. Perticaroli, J. Herzberger, Y. Sun, J. D. Nickels, R. P. Murphy, K. Weigandt, and P. J. Ray, "Multiscale microstructure, composition, and stability of surfactant/polymer foams," *Langmuir*, vol. 36, no. 48, pp. 14 763–14 771, 2020.

[36] S. P. Chaudhari and R. P. Dugar, "Application of surfactants in solid dispersion technology for improving solubility of poorly water soluble drugs," *Journal of Drug Delivery Science and Technology*, vol. 41, pp. 68–77, 2017.

[37] Z. Niroobakhsh, M. Litman, and A. Belmonte, "Flow instabilities due to the interfacial formation of surfactant–fatty acid material in a hele-shaw cell," *Physical Review E*, vol. 96, no. 5, p. 053102, 2017.

[38] Z. Niu, J. He, T. P. Russell, and Q. Wang, "Synthesis of nano/microstructures at fluid interfaces," *Angewandte Chemie International Edition*, vol. 49, no. 52, pp. 10 052–10 066, 2010.

[39] K. Kamiya, R. Kawano, T. Osaki, K. Akiyoshi, and S. Takeuchi, "Cell-sized asymmetric lipid vesicles facilitate the investigation of asymmetric membranes," *Nature Chemistry*, vol. 8, no. 9, p. 881, 2016.

[40] Y.-x. Shen, P. O. Saboe, I. T. Sines, M. Erbakan, and M. Kumar, "Biomimetic membranes: A review," *Journal of Membrane Science*, vol. 454, pp. 359–381, 2014.

[41] A. Taubert, A. Napoli, and W. Meier, "Self-assembly of reactive amphiphilic block copolymers as mimetics for biological membranes," *Current Opinion in Chemical Biology*, vol. 8, no. 6, pp. 598–603, 2004.

[42] H. K. Baca, E. Carnes, S. Singh, C. Ashley, D. Lopez, and C. J. Brinker, "Cell-directed assembly of bio/nano interfacesâa new scheme for cell immobilization," *Accounts of Chemical Research*, vol. 40, no. 9, pp. 836–845, 2007.

[43] Z. Niroobakhsh and A. Belmonte, "Dynamics of a reactive micellar oil-water interface in a flowing liquid column," *Journal of Non-Newtonian Fluid Mechanics*, vol. 261, pp. 111–122, 2018.

[44] C. Lang, J. A. LaNasa, N. Utomo, Y. Xu, M. J. Nelson, W. Song, M. A. Hickner, R. H. Colby, M. Kumar, and R. J. Hickey, "Solvent-non-solvent rapid-injection for preparing nanostructured materials from micelles to hydrogels," *Nature Communications*, vol. 10, no. 1, pp. 1–10, 2019.

[45] E. M. Herzig, K. A. White, A. B. Schofield, W. C. Poon, and P. S. Clegg, "Bicontinuous emulsions stabilized solely by colloidal particles," *Nature Materials*, vol. 6, no. 12, pp. 966–971, 2007.

[46] A. B. Subramaniam, M. Abkarian, L. Mahadevan, and H. A. Stone, "Non-spherical bubbles," *Nature*, vol. 438, no. 7070, pp. 930–930, 2005.

[47] Y. Chevalier and M.-A. Bolzinger, "Emulsions stabilized with solid nanoparticles: Pickering emulsions," *Colloids and Surfaces A: Physicochemical and Engineering Aspects*, vol. 439, pp. 23–34, 2013.

[48] J.-F. Berret, "Rheology of wormlike micelles: Equilibrium properties and shear banding transitions," in *Molecular Gels*. Springer, 2006, pp. 667–720.

[49] D. K. Schwartz, "Mechanisms and kinetics of self-assembled monolayer formation," *Annual Review of Physical Chemistry*, vol. 52, no. 1, pp. 107–137, 2001.

[50] T. L. Rodgers, O. Mihailova, and F. R. Siperstein, "Dissolution of lamellar phases," *The Journal of Physical Chemistry B*, vol. 115, no. 34, pp. 10 218–10 227, 2011.

[51] A. A. Peña and C. A. Miller, "Solubilization rates of oils in surfactant solutions and their relationship to mass transport in emulsions," *Advances in Colloid & Interface Science*, vol. 123, pp. 241–257, 2006.

[52] G. M. Whitesides and B. Grzybowski, "Self-assembly at all scales," *Science*, vol. 295, no. 5564, pp. 2418–2421, 2002.

[53] S. A. Adcock and J. A. McCammon, "Molecular dynamics: survey of methods for simulating the activity of proteins," *Chemical Reviews*, vol. 106, no. 5, pp. 1589–1615, 2006.

[54] P. Espanol and P. B. Warren, "Perspective: Dissipative particle dynamics," *The Journal of Chemical Physics*, vol. 146, no. 15, p. 150901, 2017.

[55] J. C. Shillcock and R. Lipowsky, "Equilibrium structure and lateral stress distribution of amphiphilic bilayers from dissipative particle dynamics simulations," *The Journal of Chemical Physics*, vol. 117, no. 10, pp. 5048–5061, 2002.

[56] Z. Niroobakhsh, *Viscoelastic Surfactant/Fatty Acid Interfaces: Fluid Dynamics, Rheology, and Structure*. The Pennsylvania State University, 2017.

[57] C. A. Miller, "Solubilization in surfactant systems," *Handbook of Surface and Colloid Chemistry, third ed. Taylor and Francis, Boca Raton, FL*, 2009.

[58] B.-H. Chen, C. A. Miller, and P. R. Garrett, "Rates of solubilization of triolein/fatty acid mixtures by nonionic surfactant solutions," *Langmuir*, vol. 14, no. 1, pp. 31–41, 1998.

[59] S. S. Tzocheva, P. A. Kralchevsky, K. D. Danov, G. S. Georgieva, A. J. Post, and K. P. Ananthapadmanabhan, "Solubility limits and phase diagrams for fatty acids in anionic (sles) and zwitterionic (capb) micellar surfactant solutions," *Journal of Colloid & Interface Science*, vol. 369, no. 1, pp. 274–286, 2012.

[60] K. T. Raterman, K. L. Adams, and J. A. Shaeiwitz, "Liquid solubilization dynamics: Iii. use of a quiescent technique to determine the correct boundary condition for solubilization of oleic acid in sodium taurodeoxycholate," *Journal of Colloid & Interface Science*, vol. 98, no. 2, pp. 406–419, 1984.

[61] J. J. Janke, W. D. Bennett, and D. P. Tieleman, "Oleic acid phase behavior from molecular dynamics simulations," *Langmuir*, vol. 30, no. 35, pp. 10 661–10 667, 2014.

[62] C. Huang, D. F. Evans, and E. Cussler, "Linoleic acid solubilization with a spinning liquid disc," *Journal of Colloid & Interface Science*, vol. 82, no. 2, pp. 499–506, 1981.

[63] S. R. Dungan, B. H. Tai, and N. I. Gerhardt, "Transport mechanisms in the micellar solubilization of alkanes in oil-in-water emulsions," *Colloids and Surfaces A: Physicochemical and Engineering Aspects*, vol. 216, no. 1-3, pp. 149–166, 2003.

[64] S. Soontravanich, H. E. Lopez, J. F. Scamehorn, D. A. Sabatini, and D. R. Scheuing, "Dissolution study of salt of long chain fatty acids (soap scum) in surfactant solutions. part i: equilibrium dissolution," *Journal of Surfactants and Detergents*, vol. 13, no. 4, pp. 367–372, 2010.

[65] A. Kabalnov and J. Weers, "Kinetics of mass transfer in micellar systems: surfactant adsorption, solubilization kinetics, and ripening," *Langmuir*, vol. 12, no. 14, pp. 3442–3448, 1996.

[66] P. Todorov, G. Marinov, P. Kralchevsky, N. Denkov, P. Durbut, G. Broze, and A. Mehreteab, "Kinetics of triglyceride solubilization by micellar solutions of nonionic surfactant and triblock copolymer. 3. experiments with single drops," *Langmuir*, vol. 18, no. 21, pp. 7896–7905, 2002.

[67] H. Vorum, R. Brodersen, U. Kragh-Hansen, and A. O. Pedersen, "Solubility of long-chain fatty acids in phosphate buffer at ph 7.4," *Biochimica et Biophysica Acta (BBA)-Lipids and Lipid Metabolism*, vol. 1126, no. 2, pp. 135–142, 1992.

[68] J. Clifford and B. Pethica, "The self-diffusion coefficient of sodium dodecyl sulfate micelles," *The Journal of Physical Chemistry*, vol. 70, no. 10, pp. 3345–3346, 1966.

[69] R. B. Bird, W. E. Stewart, and E. N. Lightfoot, *Transport phenomena*. John Wiley & Sons, 2006, vol. 1.

[70] T. Haliloglu and W. L. Mattice, "Monte carlo lattice simulation of the interchange of chains between micelles of diblock copolymers," *Chemical Engineering Science*, vol. 49, no. 17, pp. 2851–2857, 1994.

[71] P. Espanol and P. Warren, "Statistical mechanics of dissipative particle dynamics," *EPL (Europhysics Letters)*, vol. 30, no. 4, p. 191, 1995.

[72] R. D. Groot and P. B. Warren, "Dissipative particle dynamics: Bridging the gap between atomistic and mesoscopic simulation," *The Journal of Chemical Physics*, vol. 107, no. 11, pp. 4423–4435, 1997.

[73] A. Grafmüller, J. Shillcock, and R. Lipowsky, "The fusion of membranes and vesicles: pathway and energy barriers from dissipative particle dynamics," *Biophysical Journal*, vol. 96, no. 7, pp. 2658–2675, 2009.

[74] S.-L. Yuan, Z.-T. Cai, G.-Y. Xu, and Y.-S. Jiang, "Mesoscopic simulation study on phase diagram of the system oil/water/aerosol ot," *Chemical Physics Letters*, vol. 365, no. 3-4, pp. 347–353, 2002.

[75] D. Varade, T. Joshi, V. Aswal, P. Goyal, P. Hassan, and P. Bahadur, "Effect of salt on the micelles of cetyl pyridinium chloride," *Colloids and Surfaces A: Physicochemical and Engineering Aspects*, vol. 259, no. 1-3, pp. 95–101, 2005.

[76] J. C. Shillcock. Open source polymer research engine - dissipative particle dynamics. [Online]. Available: https://github.com/Osprey-DPD/osprey-dpd

[77] B. Duan, X. Zhang, B. Qiao, B. Kong, and X. Yang, "Description of ionic surfactant/water system by adjusting mesoscopic parameters," *The Journal of Physical Chemistry B*, vol. 113, no. 26, pp. 8854–8859, 2009.

[78] J. Bhattacharjee, V. Aswal, P. Hassan, R. Pamu, J. Narayanan, and J. Bellare, "Structural evolution in catanionic mixtures of cetylpyridinium chloride and sodium deoxycholate," *Soft Matter*, vol. 8, no. 39, pp. 10 130–10 140, 2012.

[79] C. Tanford, "Micelle shape and size," *The Journal of Physical Chemistry*, vol. 76, no. 21, pp. 3020–3024, 1972.

[80] I. Langmuir, "The constitution and fundamental properties of solids and liquids. ii. liquids." *Journal of the American Chemical Society*, vol. 39, no. 9, pp. 1848–1906, 1917.

[81] K. Morigaki and P. Walde, "Fatty acid vesicles," *Current Opinion in Colloid & Interface Science*, vol. 12, no. 2, pp. 75–80, 2007.

[82] L. Rekvig, B. Hafskjold, and B. Smit, "Chain length dependencies of the bending modulus of surfactant monolayers," *Physical Review Letters*, vol. 92, no. 11, p. 116101, 2004.

VITA

Houman Honaryar was born on September 29, 1995 in Isfahan, Iran. He attended high school at Shahid Ejei High School as a part of National Organization for Development of Exceptional Talents (NODET). After graduating high school, he started his bachelor studies at Amirkabir University of Technology (Tehran Polytechnic) pursuing a chemical engineering degree. Aside from academics and during his initial years of undergraduate education, Houman was involved in extracurricular activities and was elected as the President of Scientific Association of Chemical Engineering Department. He then was admitted to Master's program of University of Missouri - Kansas City majoring in mechanical engineering. Houman joined Dr. Niroobakhsh research group as a graduate research assistant in January 2019 and started his research work. As a graduate student, Houman was awarded the Dean's International Scholarship. Upon his graduation, he plans to continue to pursue his Ph.D. at UMKC.